NRC Research Press

ARTICLE

Geology, lithogeochemistry, and significance of porphyry intrusions associated with gold mineralization within the Timmins–Porcupine gold camp, Canada

Peter J. MacDonald and Stephen J. Piercey

Abstract: The Timmins–Porcupine gold camp, Abitibi greenstone belt, is host >60 Moz of Au with many gold deposits spatially associated with porphyry intrusions and the Porcupine–Destor deformation zone (PDDZ). Porphyry intrusions form three suites. The Timmins porphyry suite (TIS) consists of high-Al tonalite–trondjhemite–granodiorite (TTG) with calc–alkalic affinities and high La/Yb ratios and formed during ~2690 Ma D1-related crustal thickening and hydrous partial melting of mafic crust where garnet and hornblende were stable in the residue. The Carr Township porphyry intrusive suite (CIS) and the granodiorite intrusive suite (GIS) also have high-Al TTG, calc-alkalic affinities, but were generated 10–15 million years after the TIS; the CIS were generated at shallower depths (during postorogenic extension?) with no garnet in the crustal residue, whereas the GIS formed during D2 thrust-related crustal thickening and partial melting where garnet was stable in the residue. Gold mineralization is preferentially associated with the TIS, and to a lesser extent the GIS, proximal to the PDDZ. Intrusions near mineralization have abundant sericite, carbonate, and sulphide alteration. These intrusions exhibit low Na_2O and Sr, and high Al_2O_3/Na_2O, K_2O, K_2O/Na_2O, Rb, and Cs, (i.e., potassic alteration); sulfide- and carbonate-altered porphyries have high $(CaO + MgO + Fe_2O_3)/Al_2O_3$ and LOI values. Although porphyries are not genetically related to gold mineralization, they are spatially related and are interpreted to reflect the emplacement of intrusions and subsequent Au-bearing fluids along the same crustal structures. The intrusive rocks also served as structural traps, where gold mineralization precipitated in dilatant structures along the margins of intrusions during regional (D3?) deformation.

Key words: Abitibi, orogenic gold, lithogeochemistry, economic geology, petrology.

Résumé : Le camp minier de Timmins–Porcupine, dans la ceinture de roches vertes de l'Abitibi, renferme plus de 60 Moz d'or, dont de nombreux gisements aurifères associés dans l'espace à des intrusions de porphyre et la zone de déformation de Porcupine–Destor (ZDPP). Les intrusions de porphyre forment trois séries. La série de porphyres de Timmins (TIS) est composée de tonalites-trondjhémites-granodiorites (TTG) riches en Al avec des affinités calcoalcalines et des rapports La/Yb élevés et elle s'est formée vers 2690 Ma durant un épaississement crustal associé à D1 et la fusion partielle de croûte mafique en présence d'eau ayant produit des roches résiduelles dans lesquelles le grenat et la hornblende étaient stables. La série d'intrusions porphyriques du township de Carr (CIS) et la série intrusive granodioritique (GIS) présentent aussi des TTG riches en Al à affinités calcoalcalines, mais ont été produites de 10 millions d'années à 15 millions d'années après la TIS; la CIS a été générée à de plus faibles profondeurs (durant une extension post-orogénique?), le grenat n'étant pas stable dans le résidu, alors que la GIS s'est formée durant l'épaississement crustal associé au chevauchement D2 et une fusion partielle dans le résidu de laquelle le grenat était stable. La minéralisation aurifère est préférentiellement associée à la TIS et, dans une moindre mesure, à la GIS, à proximité de la ZDPP. Dans les intrusions à proximité de minéralisation, la séricite, les carbonates et une altération à sulfures sont abondants. Ces intrusions présentent de faibles concentrations de Na_2O et Sr et des valeurs élevées de Al_2O_3/Na_2O, K_2O, K_2O/Na_2O, Rb et Cs (c.-à-d., altération potassique); les porphyres à altération à sulfures et carbonates présentent des valeurs élevées de $(CaO + MgO + Fe_2O_3)/Al_2O_3$ et de perte au feu. Si les porphyres ne sont pas génétiquement reliés à la minéralisation aurifère, ils lui sont associés dans l'espace et interprétés comme reflétant la mise en place d'intrusions, puis de fluides aurifères le long des mêmes structures crustales. Les roches intrusives ont également servi de pièges structuraux dans lesquels la minéralisation aurifère a été précipitée dans des structures de dilatation le long des bordures d'intrusions durant la déformation régionale (D3?). [Traduit par la Rédaction]

Mots-clés : Abitibi, or orogénique, lithogéochimie, géologie économique, pétrologie.

Introduction

The Timmins–Porcupine gold camp represents one of the world's most prolific gold mining camps containing >60 Moz of Au (past production and current reserves) since its discovery in 1909 (Card and Poulsen 1998; Brisbin 1997; Robert and Poulsen 1997). Gold mineralization in the camp has a strong spatial association with felsic intrusive rocks, often called "porphyries" (herein termed the Porcupine intrusive suites; Fig. 1). Although most of the gold produced from the Timmins–Porcupine camp has been within 1 km of these intrusions (Fig. 2), the exact relationship of porphyries to gold mineralization remains unknown and debated (e.g., Gray and Hutchinson 2001).

The spatial association between gold mineralization and porphyry bodies has been recognized since the early days of mining

Received 10 April 2018. Accepted 19 November 2018.

P.J. MacDonald. Earth Resources and Geoscience Mapping Section, Ontario Geological Survey, 933 Ramsey Lake Road, Sudbury, ON P3E 6B5, Canada.
S.J. Piercey. Department of Earth Sciences, Memorial University of Newfoundland, St. John's, NL A1B 3X5, Canada.
Corresponding author: Stephen J. Piercey (email: spiercey@mun.ca).

Fig. 1. Regional geological map displaying the location of different assemblages of the Abitibi greenstone belt in the Timmins–Porcupine gold camp, Timmins, Canada (modified from Ayer et al. 1999*a*, 1999*b*). Map also highlights the Porcupine intrusive suites examined in this study. Coordinates are Universal Transverse Mercator (UTM), zone 17, North American Datum 1927 (NAD27). [Colour online.]

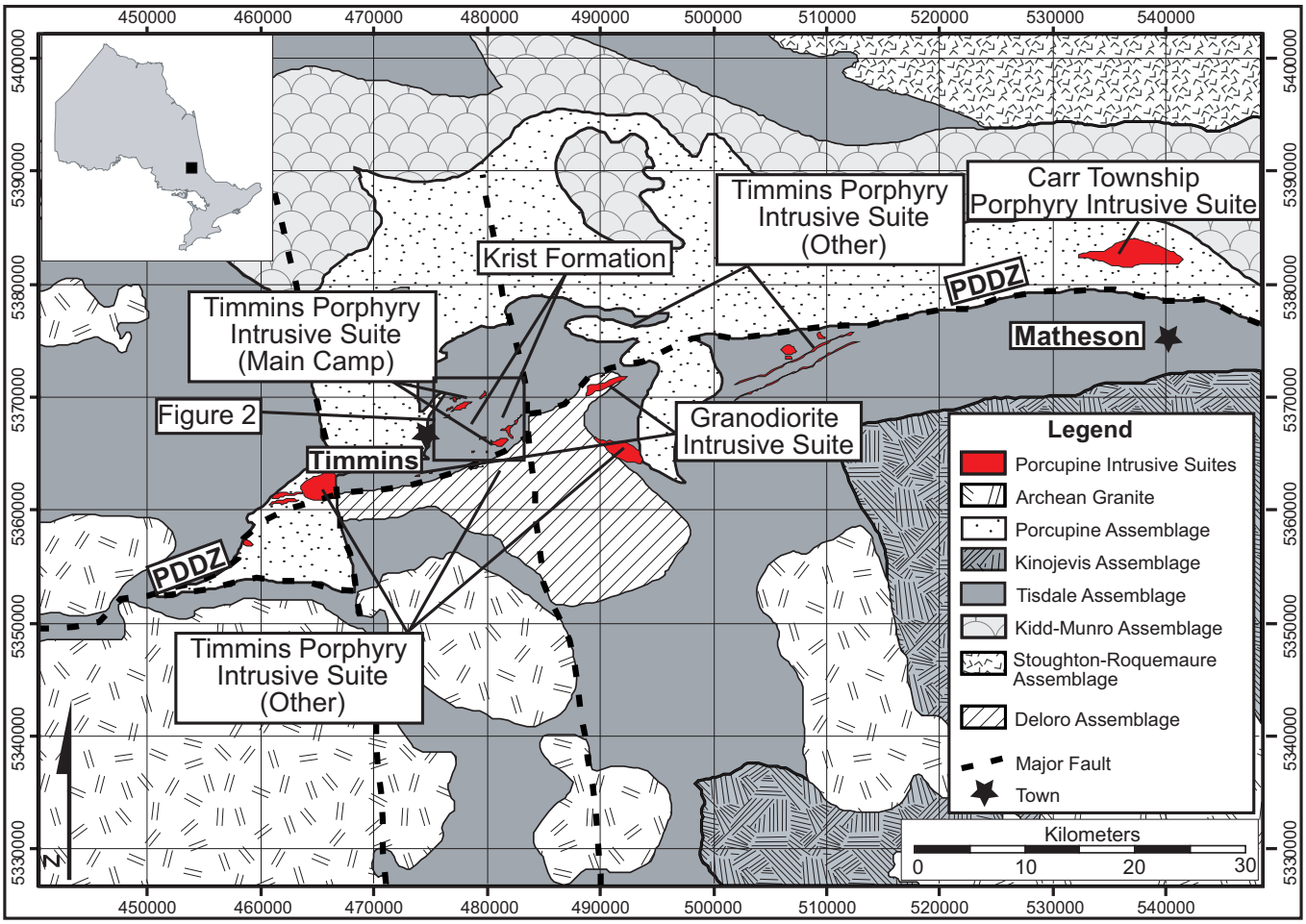

(e.g., Burrows 1925). Some workers advocated a porphyry copper model in which Au enrichment was due to magmatic–hydrothermal fluids derived from the porphyries (Mason 1986*a*, 1986*b*; Mason and Melnik 1986; Davies and Luhta 1978). Other workers illustrated that field relationships are incompatible with a porphyry model as gold mineralization was late syn- to post-tectonic, whereas the porphyry bodies were pre- to early syntectonic (Burrows and Spooner 1986; Wood et al. 1986). Wood et al. (1986), Burrows and Spooner (1986) and Burrows et al. (1993) argued that the porphyries were structural traps that allowed gold to be deposited along the margins of the porphyries during regional deformation. Coincident U–Pb zircon geochronology on the porphyries suggested that porphyries predated gold mineralization (Corfu et al. 1989; Marmont and Corfu 1989). More recently, Gray and Hutchinson (2001) argued there were two separate gold mineralization events in the Timmins–Porcupine camp: an early porphyry-related Cu–Au event (i.e., magmatic–hydrothermal) followed by a younger, structural event (i.e., orogenic) that was responsible for the bulk of the gold mineralization in the district.

In addition, the relationship between intrusive and extrusive magmatism, namely the relationship between the sulfide-bearing Krist Formation (KF) pyroclastic rocks and the Timmins porphyry intrusive suite, is uncertain within the Timmins–Porcupine gold camp. Early work suggested there were temporal differences between the Porcupine intrusive suites (~2690 Ma) and KF (~2698 Ma). Zircon geochronology (U–Pb) has shown that tuffaceous rocks of the KF contain zircons ranging from 2690 Ma to 2687 Ma, suggesting that it may be an extrusive equivalent of some of the porphyry intrusions (Ayer et al. 2003*b*). However, there have been no lithogeochemical and petrological studies to test this hypothesis.

In light of the above and despite the long-known spatial association of porphyry intrusions to gold mineralization in the Timmins–Porcupine camp, there has not been a modern, regional-scale study of the geology, geochemistry, and genesis of intrusions associated with mineralization in the camp. This paper, coupled with previously reported government research as part of the Discover Abitibi Initiative (Ayer et al. 2005), was undertaken to document the field relationships, petrology, and geochemical attributes of the Porcupine intrusive suites within the Timmins–Porcupine gold camp along the Porcupine–Destor deformation zone (PDDZ). Preliminary documentation has been presented by MacDonald and Piercey (2003), MacDonald et al. (2004), and MacDonald et al. (2005). Herein, the field relationships, petrography, and geochronological data from the above preliminary work are highlighted and summarized, whereas this manuscript focuses primarily on the lithogeochemistry of the calc-alkaline intrusive suites. The goals of this paper are: (*i*) to constrain the broader petrogenetic history of the various intrusive suites and their geodynamic setting, (*ii*) to understand their relationship(s) to coeval felsic volcanism, and (*iii*) to decipher the lithogeochemical differences between gold-associated and gold-barren intrusive rocks within the Timmins–Porcupine camp.

Fig. 2. Simplified surface geology map of the Timmins–Porcupine gold camp showing the location of some of the Porcupine intrusive suites (specifically Timmins porphyry suite - main camp) in relation to some of the more historically significant producing gold mines, the Krist Formation and Tisdale Assemblage formations (modified from Ferguson 1968; Brisbin 1997; Ayer et al. 1999*a*, 1999*b*; Hall et al. 2003). [Colour online.]

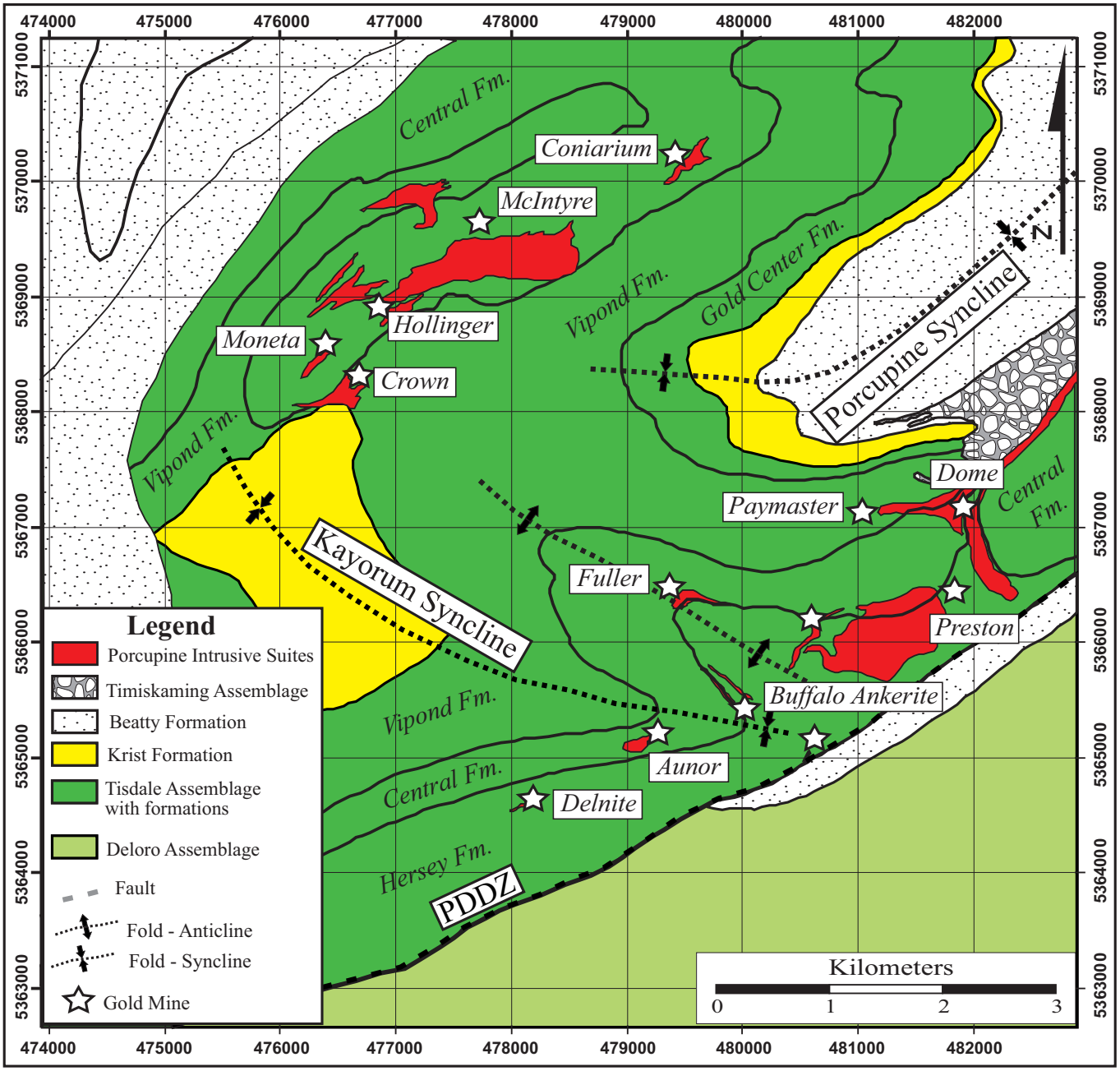

Regional geological setting

The oldest rocks in the Timmins–Porcupine gold camp are the calc-alkaline volcanic rocks of the Deloro Assemblage (2734–2724 Ma), which occur south of the PDDZ (Figs. 1 and 3) (Pyke 1982; Brisbin 1997, 2000; Bateman et al. 2008; Ayer et al. 2002, 2003*a*, 2005; Thurston et al. 2008; Dubé et al. 2017). Most gold deposits of the Timmins–Porcupine camp, however, occur north of the PDDZ within the volcanic flows of the younger Tisdale Assemblage (2710–2704 Ma; Figs. 1 and 3) (Pyke 1982; Brisbin 1997, 2000; Bateman et al. 2008; Ayer et al. 2002, 2003*a*, 2005; Thurston et al. 2008; Bleeker 2015; Dubé et al. 2017). The volcanic flows of the Tisdale Assemblage range from komatiitic at the base of the assemblage (Hersey Lake Formation) to Mg- and Fe-tholeiitic (Central, Vipond and Gold Centre formations) in the middle to upper units of the assemblage (Fig. 3) (Pyke 1982; Brisbin 1997, 2000; Bateman et al. 2008; Ayer et al. 2002, 2003*a*, 2005; Dubé et al. 2017).

The Tisdale Assemblage volcanic rocks were intruded by numerous ~2691–2687 Ma (Ayer et al. 2003*a*, 2005; Corfu et al. 1989), intermediate to felsic porphyritic intrusions (the Porcupine intrusive suite; Figs. 1 and 3) (MacDonald et al. 2005). Felsic metavolcanic rocks of the KF (~2690–2687 Ma) form the base of the Porcupine Assemblage and unconformably overlie the Tisdale Assemblage and are coeval with the porphyritic intrusions (Figs. 1 and 3) (Pyke 1982; Brisbin 1997, 2000; Ayer et al. 2002, 2003*a*, 2003*b*, 2005; Bateman et al. 2008; Thurston et al. 2008).

Postdating the intermediate to felsic porphyry intrusions and KF are clastic sedimentary rocks of the middle and upper sections of the Porcupine Assemblage, which were deposited 2690–2685 Ma

Fig. 3. Stratigraphic column for the Timmins–Porcupine gold camp, Abitibi greenstone belt. Assemblages included are the Deloro, Tisdale, Porcupine, and Timiskaming (modified from Pyke 1982; Ayer et al. 2002). Maximum thicknesses of assemblages are presented, excluding the Deloro Assemblage. Ages are from Ayer et al. (2002) and Ketchum et al. (2008). [Colour online.]

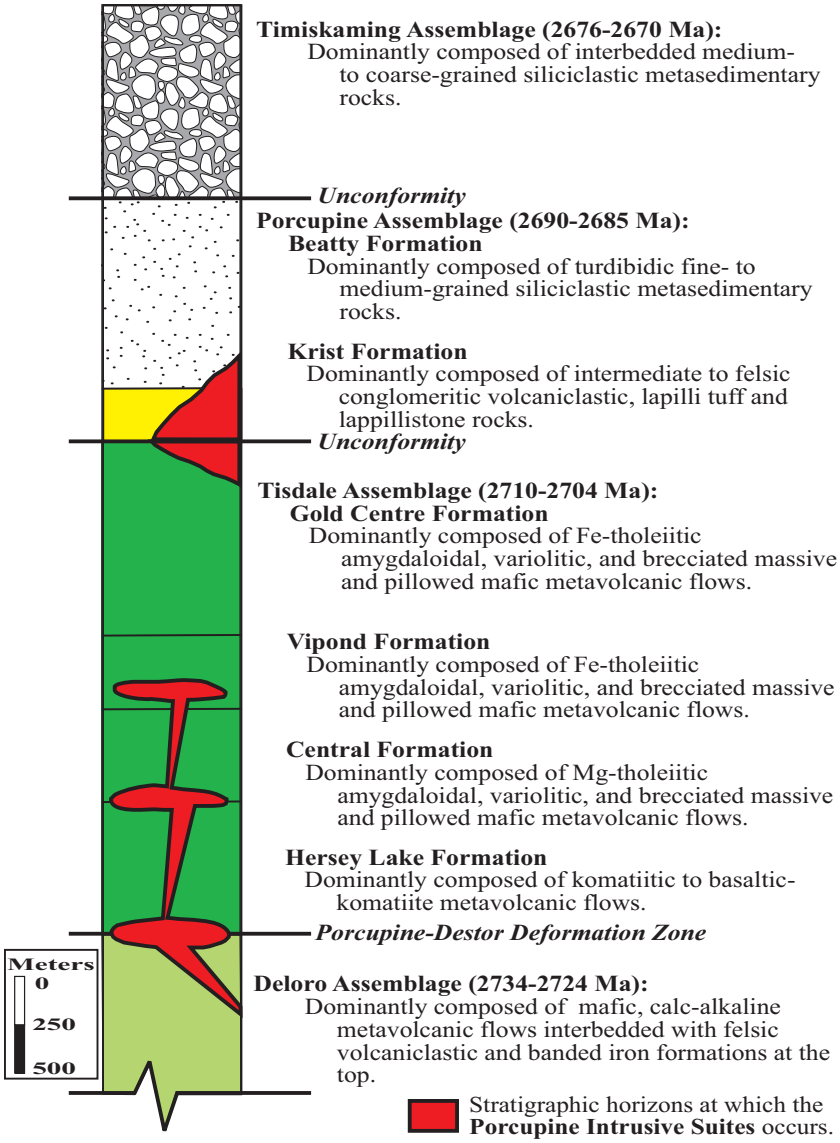

(Figs. 1 and 3) (Ayer et al. 2002, 2003*a*, 2005; Bateman et al. 2008; Thurston et al. 2008). The Porcupine Assemblage overlies the KF within fold and (or) fault controlled basins, such as the Porcupine and Kayorum synclines (Fig. 2) (Pyke 1982; Brisbin 1997, 2000; Ayer et al. 2002, 2003*a*, 2005). Coarse-grained, clastic rocks of the Timiskaming Assemblage postdate the Porcupine Assemblage and were deposited from 2679 to 2669 Ma (Brisbin 1997, 2000; Ayer et al. 2002, 2003*a*, 2005; Monecke et al. 2017).

The majority of gold in the Timmins–Porcupine camp crosscut and postdate albitite dykes that were locally emplaced at 2673 +6/–2 and 2672.8 ± 1.1 Ma (Corfu et al. 1989; Ayer et al. 2005). This is supported by recent Re-Os ages molybdenite from the Dome mine (2670 ± 10 Ma; Ayer et al. 2003*b*) and the McIntyre mine (2672 ± 7 Ma; Bateman et al. 2004). The McIntyre mine Re-Os date, however, is within error of the emplacement age of albitite dikes, suggesting some Cu–Au mineralization are temporally, and may be genetically, related to hydrothermal activity generated by albitite dike emplacement (Melnik-Proud 1992; Brisbin 1997, 2000).

Geological attributes of the Porcupine intrusive suites and KF rocks

Geological attributes of Porcupine intrusive suites

The intrusions of the Timmins–Porcupine gold camp all display near identical characteristics but are grouped into three suites based on geographic location, geology, and lithogeochemistry (MacDonald et al. 2005). The suites include the: Timmins porphyry intrusive suite (TIS), Carr Township porphyry intrusive suite (CIS), and granodiorite intrusive suite (GIS) (Fig. 1). The TIS is further subdivided into TIS-main camp and TIS-other groups by the geographical location of the individual intrusions (Fig. 1). The TIS-main camp are within the immediate vicinity of the Timmins town site, whereas TIS-other include distal porphyry intrusions, south of the PDDZ, west of the Mattagami River Fault, excluding the Bristol Township alkaline complex that occurs in and around the Timmins West mine complex, and east of the Burrows–Benedict Fault, (Fig. 1). The individual intrusions that make up each of the suites are presented on Fig. 1 and Table 1, and their geographical and

Table 1. Table of field relationships, petrology, alteration, veining, mineralization, deformation, and geochronology for the five Porcupine intrusive suites.

Category	Subcategory	TIS-main camp	TIS-other	CIS	GIS
Field Relationships	Trend	East–northeast and west–southwest	Generally east–west	East–west	East–northeast and west–southwest
	Size of trend?	Two trends: 8 × 2 km and 4 × 1.5 km	Three groups total 50+ km along PDDZ	Over 15 × 5 km	Two trends: 2 × 0.5 km 5 × 2.5 km
	Join at depth?	Yes	Yes and ???	Composite?	???
	Plunge direction?	East	West and ???	???	???
	Stratigraphic level	1. Northern margin of the PDDZ	1. Upper Deloro Assemblage and Deloro-Tisdale Assemblages contact	1. Tisdale–Porcupine Assemblages contact (lower and middle Tisdale ~Vipond Formation)	1. Upper Deloro Assemblage and Deloro–Tisdale Assemblages contact
		2. Hersey Lake–Central Formation contact	2. Hersey Lake–Central Formation contact	—	2. Hersey Lake–Central Formation contact
		3. Central and Vipond Formations (Tisdale Assemblage)	3. Base of the Porcupine Assemblage and Tisdale–Porpcupine Assemblages contact	—	—
	Stratigraphy conformable?	Generally semi-conformable	Semi-conformable	Semi-conformable?	Semi-conformable
	Other favourable zones for intrusion?	1. Pillowed mafic flows of the Tisdale Assemblage	1. Assemblage contacts	N/A	1. Fault zones (Dome fault extension and PDDZ)
		2. “Carb rock” alteration zones	2. Fault zones (PDDZ and related splays)	—	2. Fold margins (Shaw Dome?)
		3. Fault zones (e.g., Dome fault)	3. Fold margins (Shaw Dome)	—	—
		4. Fold hinges (e.g., Northern anticline)	—	—	—
	Sizes and shapes	1. Small dikes, sills, and plugs (up to 500 × 300 m)	1. Small dikes, sills, and plugs (up to 1 km × 200 m)	1. One large composite plug (over 12 × 5 km)	1. Small dikes and sills (up to 1 km × 1000 m)
		2. Dikes and sills (up to 2 × 0.5 km)	2. Large dikes and sills (up to 5 × 0.5 km)	—	2. Plug (~500 × 200 m)
		3. Large oval (~2 × 0.6 km)	3. Large thin dikes and sills (up to 5 km × 50 m)	—	3. Large elongate plug (~5 × 2 km)
		—	4. large oval (6 × 3 km)	—	—
	Margins	Generally straight and sharp with small apophyses	Generally straight and sharp with small apophyses	Generally straight and sharp (primary or tectonic)	Generally straight and sharp (primary or tectonic)
		Lesser marked by breccias (Edwards, Paymaster, and Crown)	Lesser marked by breccias (Bristol Township and Mt. Logano porphyries)	Lesser marked by breccia	—
		—	Minor gradational contacts (Aquarius porphyry)	—	—
Petrology	Texture	Aphanitic and porphyritic	Porphyritic	Porphyritic	Porphyritic and equigranular
	Phenocrysts	Sub- to euhedral plagioclase and quartz up to 8 mm	Sub- to euhedral plagioclase and quartz up to 6 mm	Sub- to euhedral plagioclase and quartz up to 15 mm	Sub- to euhedral plagioclase and quartz up to 6 mm
	Matrix	Aphanitic to very fine grained	Very fine grained	Fine grained	Fine grained
	Minor Minerals	Apatite and tourmaline	Apatite and tourmaline	N/A	Biotite, muscovite, and apatite
	Sulphides	Pyrite, chalcopyrite, pyrrhotite, molybdenite, and bornite	Pyrite, chalcopyrite, pyrrhotite, and molybdenite	Pyrite and chalcopyrite	Pyrite
	Foreign clasts	Green mica and porphyry fragments up to 10 cm	Green mica and porphyry fragments up to 10 cm	Rounded porphyry fragments	N/A
	Metamorphic minerals	Stilpnomelene	Biotite, chlorite, and muscovite	Trace chlorite and biotite	Biotite, chlorite, and muscovite

Table 1 (*concluded*).

Category	Subcategory	TIS-main camp	TIS-other	CIS	GIS
Alteration, veining, and mineralization	Alteration	White mica (sericite), calcium carbonate, hematite, iron-carbonate (ankerite), chlorite, and tourmaline	Sericite, calcium-carbonate, chlorite, hematite, iron-carbonate (ankerite), silicification, and albite	Sericite, chlorite, hematite, and silicification	Sericite, calcium-carbonate, chlorite, and iron-carbonate (ankerite)
	Veining	Quartz–tourmaline, quartz–ankerite, quartz–calcite, and quartz	Quartz sweats, quartz–calcite, and quartz–ankerite	Quartz sweats and quartz–calcite	Quartz sweats and quartz–calcite
	Mineralization	Gold mineralization	Gold mineralization	Anomalous gold	Gold mineralization
		Copper mineralization	Anomalous copper	Anomalous copper	No copper known
Deformation	Deformation	D2 foliation, D3 spaced cleavage, D? stretching lineation, and D6 foliation	D2 foliation and D3 spaced cleavage	D3 foliation	D3 foliation
Geochronology*	Geochronology	Paymaster = 2690 ± 2 Ma (1)	Bristol Township = 2687.7 ± 1.4 Ma (3)	Unknown; suspected ~2685–2670 Ma	Pamour = 2677.5 ± 1 Ma (4)
		Preston = ca. 2690 Ma (1)	Mt. Logano = 2689.0 ± 1.4 Ma (4)	—	—
		Dome Fault Zone = 2688 ± 2 Ma (2)	Hoyle Pond = 2684.4 ± 1.9 Ma (5)	—	—
		Crown = 2688 ± 2 Ma (1)	Hoyle Pond sill = 2687.2 ± 2.2 Ma (6)	—	—
		Millerton = 2691 ± 3 Ma (1)	Aquarius = 2705 ± 10 Ma (1)	—	—
		Pearl Lake = 2689 ± 1 Ma (1)	—	—	—
Porphyry intrusions included in study without geochronology		Miller Lake, Northern, Acme, Gillies Lake, Coniaurium, West, Northwest, Edwards, Buffalo Ankerite, and Buffalo Ankerite #5	Bristol Lake, South Bristol Lake, northern Deloro Township dike swarm, Aquarius, Homestead, Crowley, and Pominex	Carr Township	Naybob, Porphyry Hill granodiorite, and Bob's Lake granodiorite

Note: TIS, Timmins porphyry intrusive suite; CIS, Carr Township porphyry intrusive suite; GIS, granodiorite intrusive suite; and PDDZ, Porcupine–Destor deformation zone.
*Data sources for U–Pb ages are indicated as follows: (1) Corfu et al. 1989, (2) Gray and Hutchinson 2001, (3) Ayer et al. 2003, (4) MacDonald et al. 2005, (5) Bateman et al. 2005, and (6) Ayer et al. 2005.

geological relationships, petrography, metamorphism, alteration, deformation, veining, emplacement ages, and association to mineralization are summarized in Table 1.

All of the intrusive suites consist of three or more intrusions generally trending east–west, with sill-, dike-, and plug-like forms, with individual intrusions ranging from metre- to kilometre-scale (Figs. 1 and 2). The intrusions are generally sub-parallel to the volcanic stratigraphy at four discrete stratigraphic levels: (*i*) the upper units of the Deloro Assemblage, (*ii*) at the contact between the Deloro and Tisdale Assemblages, (*iii*) within the lower to middle units of the Tisdale Assemblage, and (*iv*) at the contact of the Tisdale and Porcupine Assemblages (Fig. 3). The intrusive suites are located near or at assemblage, formation, or flow contacts (Fig. 3) and have sharp, unchilled intrusive or fault contacts with wall rocks (Figs. 4A–4B). The Bristol Township and Mt. Logano porphyries of the TIS-other suite and the entire CIS are exceptions to the above and are large composite intrusive bodies instead of multiple small intrusions.

All of the intrusive suites are porphyritic, containing 5–60 vol %, subeuhedral and lesser anhedral phenocrysts of Na-rich plagioclase (oligoclase to albite) and lesser, variably strained quartz. Igneous phenocrysts are 1–15 mm in diameter and are set in massive, fine- to very fine-grained matrices of plagioclase and quartz, along with trace amounts of muscovite, chlorite, orthoclase, biotite, apatite, actinolite, leucoxene, and zircon (Figs. 4C–4D). Some intrusions of the GIS suite are equigranular, containing interlocking crystals of Na-rich plagioclase, quartz, and muscovite and biotite (Fig. 4E). Centimetre-scale xenoliths of altered ultramafic to mafic rocks are present in most intrusions. Breccias found within some porphyries are locally tourmaline-rich, but these breccias are relatively rare (Fig. 4F).

The majority of intrusions display alteration on a decimetre- to metre-scale that is found within high strain zones (Fig. 5). Sericite alteration of plagioclase crystals is the most common alteration with phenocrysts ranging from fresh to completely replaced by fine-grained sericite–muscovite (Figs. 4G–4H). In the immediate vicinity of the largest gold deposits (e.g., Hollinger–McIntyre and Dome mines), sericite alteration is most intense and is often coupled with pervasive calcium carbonate alteration (Figs. 4I and 5). Pervasive albite alteration is common along the same structures that host sericite alteration (i.e., Dome fault). Locally occurring with albite alteration is patchy iron-carbonate (ankerite), pervasive pink hematite, and strongly pervasive quartz alteration. Minor, pervasive chlorite and trace biotite alteration is also present within some intrusions. The sericite–muscovite and biotite in the intrusions increases in proximity to mineralization, suggesting the majority of the micas are hydrothermal in origin.

Regional metamorphism in the vicinity of the intrusions is lower to middle greenschist facies (Thompson 2002). Metamorphic assemblages within the intrusions include chlorite, muscovite, and biotite (after plagioclase phenocrysts and hydrothermal chlorite sericite).

All intrusions typically display two structural fabrics (Figs. 4I–4J), although the intensity of deformation varies between intrusions and intrusive suites. The two dominant structural fabrics are subparallel, generally east–west trending, near vertical, millimetre-spaced cleavages, with the former being crenulated by the latter (Figs. 4I–4J; D2 and D3) (Bateman et al. 2008). A younger, near vertical, foliation is also present in some intrusions (D6) (Bateman et al. 2008), as is a younger flat-lying foliation and conjugate sets of centimetre-sized kink folds (D7) (Bateman et al. 2008).

Multiple sets of veins cross-cut the different intrusive suites including quartz, quartz–tourmaline (Fig. 4K), quartz–ankerite, and quartz–calcite. Smaller stringer veinlets of tourmaline also occur within some of the intrusions.

The majority of TIS intrusions were emplaced between 2687 and 2691 Ma (Table 1) (Marmont and Corfu 1989; Corfu et al. 1989; MacDonald et al. 2005; Ayer et al. 2002, 2003*b*, 2005). Exceptions

Fig. 4. Photographs and photomicrographs showing key features of the Timmins–Porcupine intrusive suites and the Krist Formation: (A) sharp contact between a porphyry dike and host mafic volcanic rocks, Shaw Dome, Deloro Township; (B) 2-m-long structurally transposed dike off of larger porphyry intrusions, north Vedron property; (C) porphyritic texture with feldspar and quartz phenocrysts within a quartzo–feldspathic matrix, Gillies Lake porphyry; (D) porphyritic texture with quartz and feldspar phenocrysts within a quartzo–feldspathic matrix, Naybob porphyry, XPL; (E) equigranular texture of interlocking feldspars and quartz crystals, Porphyry Hill, XPL; (F) porphyry diatreme with sericite and hematite altered fragments of porphyry within a tourmaline-rich matrix, Pearl Lake porphyry; (G) relict feldspar phenocrysts that have undergone partial sericite replacement (alteration), Preston porphyry, XPL; (H) complete sericite replacement (alteration) of feldspar phenocrysts yielding quartz-sericite schist, Preston porphyry, XPL; (I) strongly sericite-calcium carbonate ("dirty") altered porphyry with feldspar phenocrysts completely replaced displaying D2 and D3 spaced cleavages, Pearl Lake porphyry, PPL; (J) well-developed D2 and D3 spaced cleavages, Buffalo Ankerite #5 porphyry; (K) quartz–tourmaline vein, Edwards porphyry; (L) large sulfide (pyrite) cluster (near white arrow) in Carr Township porphyry; (M) mafic clasts within a conglomerate facies of the Krist Formation, Kayorum Syncline; and (N) elongate, stretched porphyry clasts along transposed S0/S2 fabric, Krist Formation, Kayorum Syncline. XPL, cross-polarized light; PPL, plane polarized light. [Colour online.]

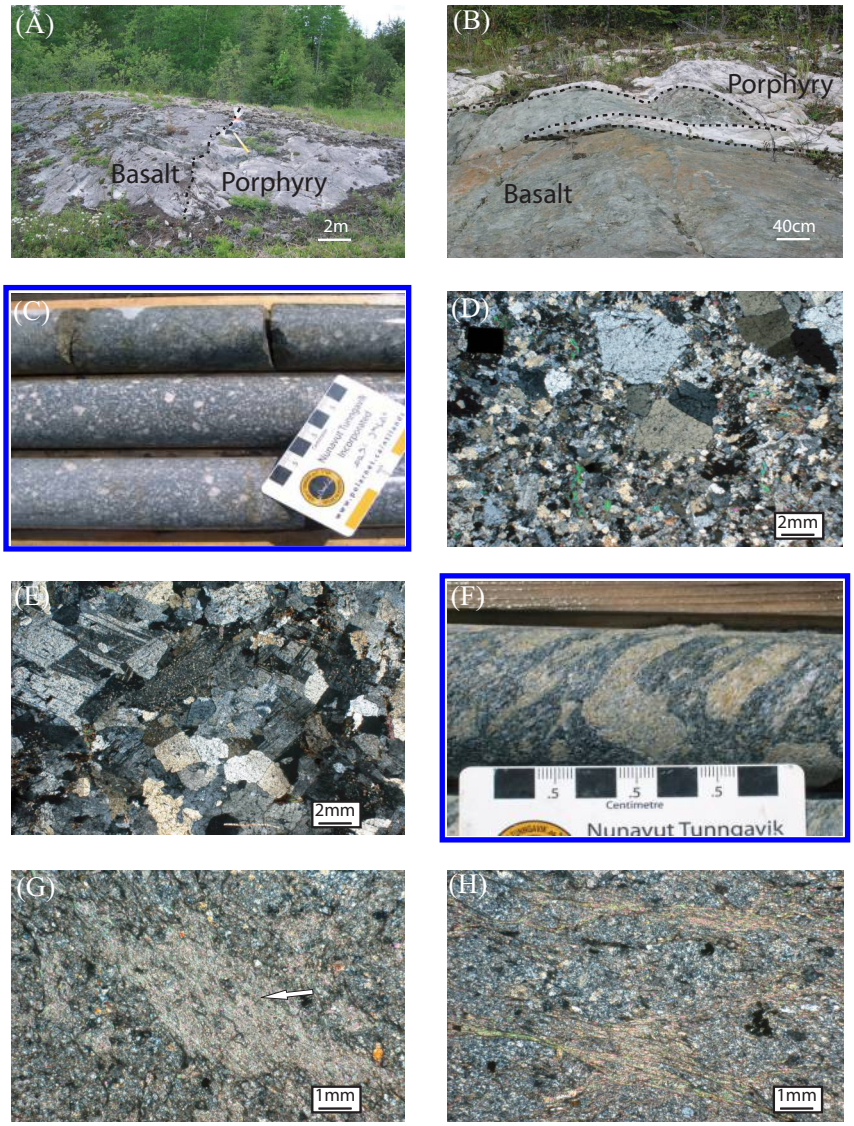

include the Hoyle Pond (2684 ± 1.9 and 2687.2 ± 2.2 Ma) and Aquarius intrusions (2705 ± 10 Ma: Table 1) (Corfu et al. 1989; Bateman et al. 2005; Ayer et al. 2005). The GIS intrusions were emplaced at 2677.5 ± 2.0 Ma (Table 1) (Ayer et al. 2005; MacDonald et al. 2005). The CIS has no U–Pb zircon ages, but is hypothesized to be younger than the TIS, as they lack a D2 fabric and have geological similarities to circa 2685-Ma potassic, calc-alkaline plutons throughout the Abitibi (Corfu et al. 1989; Davis et al. 2000; Ayer et al. 2002). When compared with regional suites documented by Beakhouse (2011) throughout the Abitibi, the TIS intrusions are interpreted to be mostly related to the 2691–2685 Ma early syntectonic suite; the GIS and CIS intrusions are related to the 2686–2676 Ma syntectonic suite.

Gold and Cu mineralization in the porphyries is associated with sub-millimetre to centimetre scale sub-euhedral disseminated grains, grain clusters (Fig. 4L), and (or) veinlets of pyrite, pyrrhotite, chalcopyrite, and bornite, and are associated with hydrothermal alteration and quartz veining. Anomalous Au (>0.05 ppm) is associated with all of the intrusive suites. Intense sericite and calcite alteration of the intrusions occurs in the vicinity of large tonnage gold mineralization (Hollinger, McIntyre, and Dome deposits) (e.g., Fig. 5), and moderately intense ankerite-sericite alteration is

Fig. 4 (*concluded*).

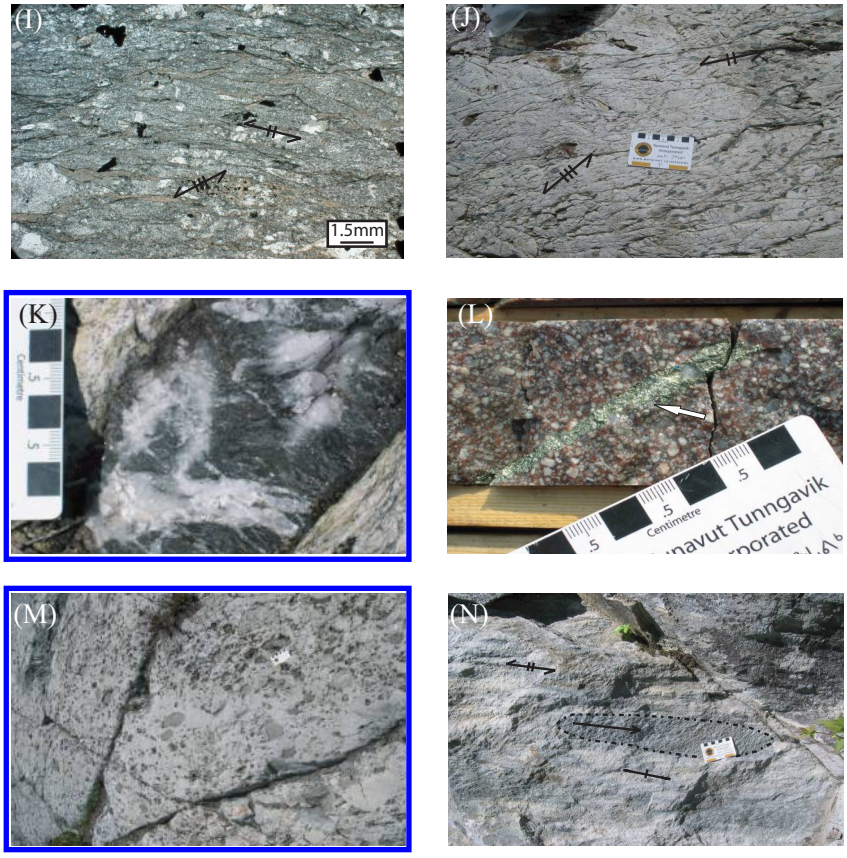

Fig. 5. Map showing structural control (Hollinger shear zone) of Hollinger–McIntyre gold mineralization and sericite ± calcium carbonate alteration (modified from Mason and Melnik 1986). [Colour online.]

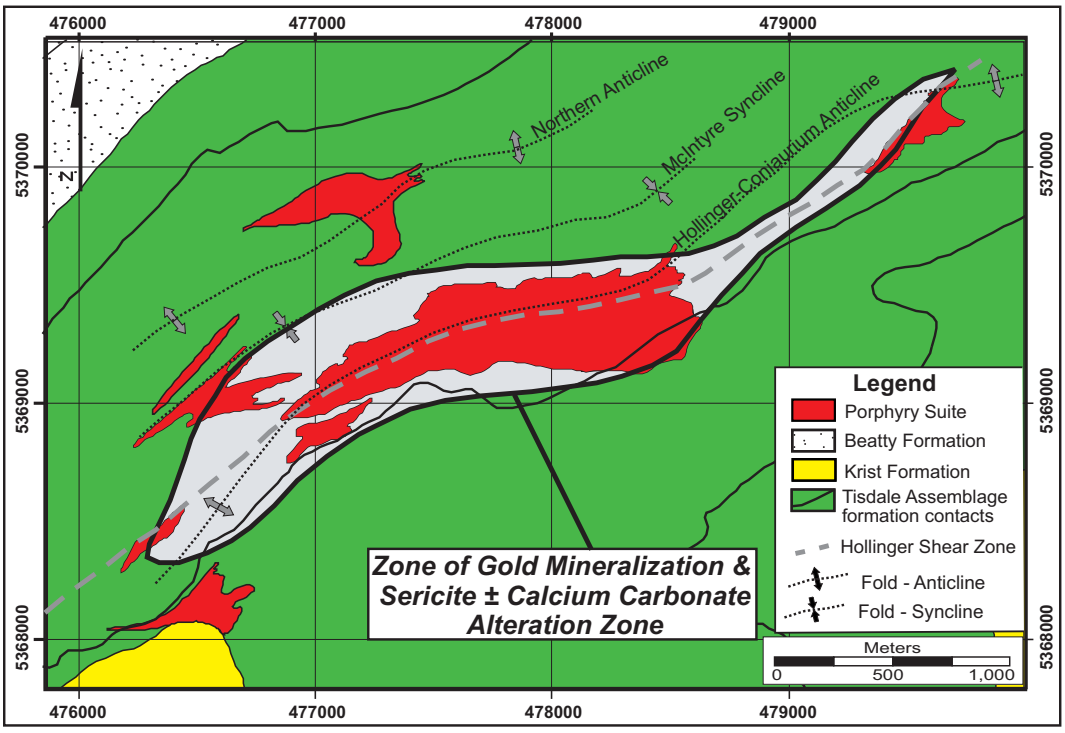

the dominant alteration proximal to smaller deposits (Paymaster 2–3, Buffalo Ankerite and Aquarius). Anomalous Cu (>1000 ppm) is associated with hematite alteration in the larger intrusions (the Pearl Lake porphyry – TIS-main, the Bristol Township porphyry – TIS-other and the Carr Township porphyry – CIS).

Geological characteristics of the KF

The KF forms the base of the Porcupine Assemblage within the Kayorum and Porcupine synclines, lying unconformably above the Tisdale Assemblage (Figs. 2–3). Ranging up to 500 m thick, the intermediate to felsic metavolcaniclastic rocks of the KF are composed of poorly sorted and bedded lapilli- to breccia-sized fragments in a quartzo–feldspathic crystal–tuff matrix (Figs. 4M–4N) (Bateman et al. 2008). The fragments are dominantly felsic with minor fragments of basalt, massive sulfide (pyrite and lesser chalcopyrite), and iron formation. The matrix is composed predominantly of plagioclase with lesser quartz and trace chlorite, orthoclase, pyrite, and zircon crystals. Pervasive, weak to moderate hydrothermal alteration is common, and typically includes sericite ± calcium carbonate and (or) albite alteration as well as with very weak, localized iron-carbonate, chlorite, quartz, and fuchsite alteration. Greenschist metamorphism of the KF is identified by the presence of minor muscovite and chlorite, presumably after hydrothermal sericite and chlorite. Deformation of the KF includes two subparallel, generally east–west trending, near vertical, millimetre-spaced cleavages with the earlier fabric crenulated by the later (D2 crenulated by D3), along with a later stretching lineation observed in stretched fragments (D5; Fig. 4N) (Bateman et al. 2008). Veins are rare within the KF and are restricted to quartz veinlets. U–Pb zircon ages from the KF range from 2687.3 ± 1.6 Ma to 2687.5 ± 1.3 Ma (Ayer et al. 2002, 2003*b*, 2005). No mineralization is known to exist in the KF.

An indirect correlation between the KF and the Porcupine intrusive suites exists, even though there is no physical link between the two units. The KF is proximal (<1 km) to many of the TIS intrusions (Fig. 2), they share many petrographic similarities, and have similar U–Pb ages, which indicate the deposition of the KF and the emplacement of the TIS were coeval ~2688 Ma (Ayer et al. 2003*b*).

Lithogeochemistry

Previous lithogeochemical studies

Few comprehensive, publically available lithogeochemical data sets exist for the Porcupine intrusive suites. Davies and Luhta (1978), Mason and Melnik (1986), Wood et al. (1986), Burrows and Spooner (1986, 1989), Burrows et al. (1993), Brisbin (2000), and Gray and Hutchinson (2001) focused on gold mineralization, but few discussed the lithogeochemistry of the intermediate to felsic porphyry intrusions. Davies (1980) showed that K–Rb enrichment is associated with sericite alteration proximal to the porphyries. McAuley (1983) studied TIS intrusions near the Dome Mine and showed that they had calc-alkaline affinity and major element lithogeochemistry indicated that the Preston, Preston West, and Paymaster porphyries were genetically related. McAuley (1983) noted K–Rb enrichment coupled with Sr depletion in sericite-altered samples and Sr enrichment with Ca, Fe, and Mg depletions in albite-altered samples. Gorman et al. (1981) suggested that the alteration of the intrusions began as sodic (Na) and evolved into potassic (K) alteration, whereas McAuley (1983) noted that sericite alteration preceded or was coeval with regional deformation and that albite alteration postdated it. Despite mineralogical variations, Wells (2001) found that both quartz–feldspar and feldspar porphyries in the vicinity of the Dome mine were coeval and genetically related. More recently, Israr (2017) undertook a melt inclusion and lithogeochemical study on the Paymaster, Crown, and Pearl Lake porphyries and the Krist fragmental unit and showed similar geochemical signatures to MacDonald et al. (2005), but also illustrated that these rocks had Cu–Au-enriched melt inclusions.

Sampling and analytical procedures

Samples of the Porcupine intrusive and KF were collected from surface exposures and drill core in 2003 and 2004. A total of 116 samples from 28 intrusive bodies and 2 KF units were collected. Each individual sample was approximately 3–5 kg. Weathered surfaces were removed and all samples were then crushed using a steel jaw crusher. Pulverization was done in an agate mortar in 2003 at the Ontario Geoscience Laboratory (GeoLabs) in Sudbury, Ontario, and a mild (carbon) steel in 2004 at Activation Laboratories Limited (ActLabs) in Ancaster, Ontario. These powders were then analyzed utilizing wavelength-dispersive X-ray fluorescence spectrometry (XRF), inductively coupled plasma atomic emission spectroscopy (ICP-ES) and inductively coupled plasma mass spectrometry (ICP-MS) at a combination of GeoLabs and ActLabs in 2003 and 2004. Major elements (SiO_2, TiO_2, Al_2O_3, Fe_2O_3T, MnO, MgO, CaO, Na_2O, K_2O, and P_2O_5) were determined on fused discs by XRF. Loss-on-ignition (LOI) was determined using conventional heating and weight difference methods. Some trace elements were determined by pressed pellet XRF analysis at the GeoLabs in 2003 (Nb, Zr, and Y) and ActLabs in 2004 (Ni, Cr, V, Nb, Zr, and Y). Other trace elements were determined by ICP-ES (Ba, Be, Cd, Co, Cr, Cu, Li, Mo, Ni, S, Sc, Sr, V, W, and Zn) and ICP-MS (Nb, Ta, Zr, Hf, Y, Cs, Th, U, La, Ce, Pr, Rb, Nd, Sm, Eu, Gd, Tb, Dy, Ho, Er, Tm, Yb, and Lu) at the GeoLabs in both 2003 and 2004 utilizing closed-beaker multi-acid digestion prior to analysis (Burnham et al. 2002; Burnham and Schweyer 2004). Analytical results are presented in Supplementary Table1[1].

Completeness of digestion during ICP-ES and ICP-MS analysis was tested by comparing duplicate elements (Ni, Cr, V, Nb, Zr, and Y) via the solid-source XRF method versus those obtained by solution ICP-ES and ICP-MS. Values obtained by XRF are within 10% of values obtained by ICP-ES and ICP-MS, suggesting digestions were complete. As such, ICP-ES (Ni, Cr, and V) and ICP-MS (Nb, Zr, and Y) trace element data are used in this paper for consistency in the data set and because of the superior detection limits and sensitivity, particularly for the rare earth elements (REE) and high field strength elements (HFSE).

Precision was calculated using the percent of relative standard deviation (%RSD) of replicate analysis of known and unknown reference materials as well as analytical duplicates. Precision for major elements (including LOI) obtained via fused disc XRF methods is < ±5% RSD with the exception of MgO and P_2O_5 (±7% RSD and ±10% RSD, respectively) from 2003 GeoLabs' analyses and K_2O (±10% RSD) from 2004 ActLabs' analyses. Precision for trace elements obtained via pressed pellet XRF were < ±10%RSD for both 2003 and 2004 analyses at GeoLabs and ActLabs. Precision for trace elements obtained via ICP-ES were generally < ±15%RSD with the exception of Cd, Mo, S, and W, which are not considered precise. Precision for trace and REE obtained via ICP-MS were <±12%RSD. For more detailed information regarding the precision of the data set presented within refer to Appendix A of MacDonald et al. (2005).

Accuracy was determined using the percent of relative difference (%RD) of reference materials of known or accepted values. Accuracy for major elements (including LOI) obtained via fused disc XRF methods and trace elements obtained from pressed pellet XRF is generally < ±10%RD from both 2003 GeoLabs' and 2004 ActLabs' analyses. Accuracy for trace elements obtained via ICP-ES and ICP-MS were generally acceptable (< ±10% RD) with the excep-

[1]Supplementary data are available with the article through the journal Web site at http://nrcresearchpress.com/doi/suppl/10.1139/cjes-2018-0091.

tion of Cd, Mo, S, and W, which are not considered accurate. For more detailed information regarding the accuracy of the methods used see Appendix A in MacDonald et al. (2005).

Alteration geochemistry and tests for immobility of immobile elements

Every attempt was made to minimize the effects of hydrothermal alteration in the data set, but most units studied are variably altered. Most of the samples exhibit variability in the major elements forming an array on an alteration box plot (Large et al. 2001) in Fig. 6A. While this diagram was constructed for volcanogenic massive sulphide deposits, the data arrays and indexes reflect alteration minerals present in a rock, which are in many cases independent of deposit type (e.g., Ahmed et al. 2019); thus, it is appropriate for illustrating alteration mineral distributions in the samples presented herein. On this plot, the samples form an array from the albite portion of the diagram towards the chlorite–pyrite node (Fig. 6A). Notably, these variations are greatest in the TIS with samples from the CIS and GIS lying primarily within the least altered rhyolite box (Fig. 6A). The samples from the TIS-main camp lie closer to the pyrite–chlorite node of the diagram, whereas the TIS-other are closer to the albite node, consistent with those near the Timmins area being more altered (Fig. 6A). The alkali mobility is also shown in Al_2O_3/Na_2O–Na_2O space, where many samples, particularly those of the TIS-main camp, have high Al_2O_3/Na_2O values (>10) and low Na_2O contents, whereas others have elevated Na_2O contents (>5%), particularly the TIS-other and some of the GIS, and only a few samples have least-altered compositions (Fig. 6B). The data form an array in K_2O–Na_2O space consistent with varying Na- and K-alteration (Fig. 6C).

To monitor carbonate alteration, $(CaO + MgO + Fe_2O_3)/Al_2O_3$ is plotted against LOI (Fig. 6D). The $(CaO + MgO + Fe_2O_3)/Al_2O_3$ is chosen as this ratio increases with increasing carbonate (and Fe sulfide) alteration as Ca–Mg–Fe will be enriched in carbonates at the expense Al_2O_3, which will be enriched in clay alteration over carbonate alteration; LOI is chosen as this is a measure of hydration (i.e., clays), carbonate, and sulfide addition (Fig. 6D). This diagram has two key trends. The first trend is a positive relationship between $(CaO + MgO + Fe_2O_3)/Al_2O_3$ and LOI, consistent with increased carbonate alteration. This trend is particularly pronounced for the TIS-main samples and a subset of the TIS-other, whereas the CIS and GIS samples have low $(CaO + MgO + Fe_2O_3)/Al_2O_3$ values (Fig. 6D). The second trend is that TIS-other samples cluster close to LOI~10, as does a subset of GIS; most of these samples have low $(CaO + MgO + Fe_2O_3)/Al_2O_3$ values (Fig. 6D), which is consistent with albite and white mica alteration with minimal carbonate addition.

It is notable that the light field strength elements (LFSE) also have been affected by alteration (Figs. 6E–6F), with Rb (and Cs, not shown) having a positive correlation with K_2O content, consistent with enrichment due to potassic metasomatism (Fig. 6E). Although less systematic, there is also a broad association of high LOI with elevated Sr, similar to the carbonate index above (Fig. 6D), suggesting potential carbonate control on Sr contents with Sr^{2+} substitution for Ca^{2+} in the carbonate minerals the likely mechanism (Fig. 6F). The exception to this, however, is a subset of the GIS, which has high Sr and low LOI contents, suggesting that the high Sr in the GIS is a primary signature in these samples (Fig. 6F), likely due to the presence of unaltered feldspars.

The above data clearly point to alkali mobility and mobility of carbonate-associated elements in the Porcupine intrusive suites. It is uncertain, however, whether or not the typically immobile elements have remained immobile, in particular the HFSE, REE, Al_2O_3, and TiO_2. This is particularly critical as these elements can be mobilized during intense alteration (e.g., Campbell et al. 1984; Murphy and Hynes 1986; Migdisov et al. 2016), which affected some samples in the data set. Furthermore, these data are utilized extensively to understand the primary petrology of ancient rock suites; therefore, establishing their mobility or immobility is critical. To test for immobility of these elements select, certain intensely altered samples were compared with analyses of a coeval least altered intrusion. The least altered samples from different Porcupine intrusive suites were chosen based on field (i.e., fresh), petrographic (i.e., preserved primarily mineralogy), and mobile element systematics (i.e., undisturbed alkalis, low LOI, alteration index, and metal values). Three typical examples of alteration types affecting TIS samples were chosen to represent the range of alteration present in the data set, namely potassic alteration (sericite-K-feldspar-biotite) with chalcopyrite and pyrite, albite alteration, and carbonate alteration (Figs. 7A–7C). One sample was chosen from both CIS and GIS to represent albite alteration and one weakly altered sample was chosen from the KF (Figs. 7D–7F). These samples were then compared with the least altered samples of their respective intrusive suites, with the exception of the KF sample, which was compared with the least altered TIS sample, using the modified isocon method (Grant 1986) of Huston (1993). While there are a number of suites in the Porcupine intrusive suite, many have similar trends in "immobile" element diagrams (e.g., Fig. 8); thus, they can be treated as coming from a limited number of single precursors. Correspondingly, the single precursor isocon method is sufficient to illustrate the mobility–immobility of elements in this study.

Results of the isocon analysis are shown in Fig. 7. On these diagrams elements that have been immobile form a line of equal concentration, the isocon, whereas elements that lie off of this line have either been gained (above the line) or lost (below the line) during the alteration process (Grant 1986). With the exception of carbonate alteration, the linearity of the HFSE, REE, and Al_2O_3, suggests that these elements have been relatively immobile during alteration (Fig. 7). Furthermore, these elements show linear trends on binary plots of immobile elements, with minor exceptions (Fig. 8) (e.g., Barrett and MacLean 1994; Barrett and MacLean 1999), and coherent trends on immobile element-based trace element plots (Figs. 9–11), suggesting they were immobile. The isocons in most samples are best defined by the HFSE (Zr, Hf, Ta, Nb, Th), and Al_2O_3, with the results illustrating most major elements and LFSE have significant gains and losses associated with the various alteration types (Fig. 7). The transition elements have variable behavior with the base metals Cu, Zn, and Pb exhibiting variable mobility, whereas others like V, Sc, and Ni appear to have been immobile (Fig. 7). The carbonate-altered samples also exhibit linear trends with the HFSE and Al_2O_3, but there are enrichments in heavy REE (Figs. 7C and 7F), and one sample exhibits TiO_2 enrichment (Fig. 7F), suggesting potential minor mobility of these elements in carbonate-altered samples (Figs. 7C and 7F). That being stated, however, the enrichment is minor, and inter-REE ratios are largely unaffected (Fig. 7).

Taken together these results suggest that the HFSE, REE, Al_2O_3 and, to a lesser extent, TiO_2 have been immobile during alteration and these elements can be utilized to understand the primary igneous compositions of the Porcupine intrusive suites.

Immobile element lithogeochemistry of the Porcupine Intrusive Suites and KF

TIS

The TIS suite has subalkalic to weakly alkalic affinities with Nb/Y~7 and dacitic to rhyolitic Zr/TiO_2 ratios (Figs. 8 and 9). The samples have Zr/Y > 4.5, Zr/Nb ~30, and Th/Yb >0.85, consistent with them having calc-alkalic affinities (Figs. 8 and 9) (Barrett and MacLean 1994; Barrett and MacLean 1999; Ross and Bedard 2009). Most samples have high Al_2O_3 and relatively low Yb contents, consistent with high-Al tonalite–trondhjemite–granodiorite (TTG) affinities (Fig. 9C), coupled with very high La/Yb values that are

Fig. 6. Mobile element plots for the Porcupine intrusive suites and the Krist Formation, including: (A) alteration boxplot (from Large et al. 2001) with Hashimoto alteration index [(MgO + K_2O)/(MgO + K_2O + Na_2O + CaO)] (Saeki and Date 1980; Date et al. 1983) plotted against chlorite–carbonate–pyrite index [(MgO + Fe_2O_3T)/(MgO + Fe_2O_3T + Na_2O + CaO)]; (B) Na_2O versus Al_2O_3/Na_2O plot with designations for least altered samples (modified from Spitz and Darling 1978); (C) Na_2O versus K_2O plot; (D) LOI versus (CaO + MgO + Fe_2O_3T/Al_2O_3 plot; (E) K_2O versus Rb plot; and (F) LOI versus Sr plot. All values are in weight percent. Alteration indexes are ratios of major elements in weight percent form. TIS, Timmins porphyry intrusive suite (main camp and other); CIS, Carr Township porphyry intrusive suite; GIS, granodiorite intrusive suite; and KF, Krist Formation. [Colour online.]

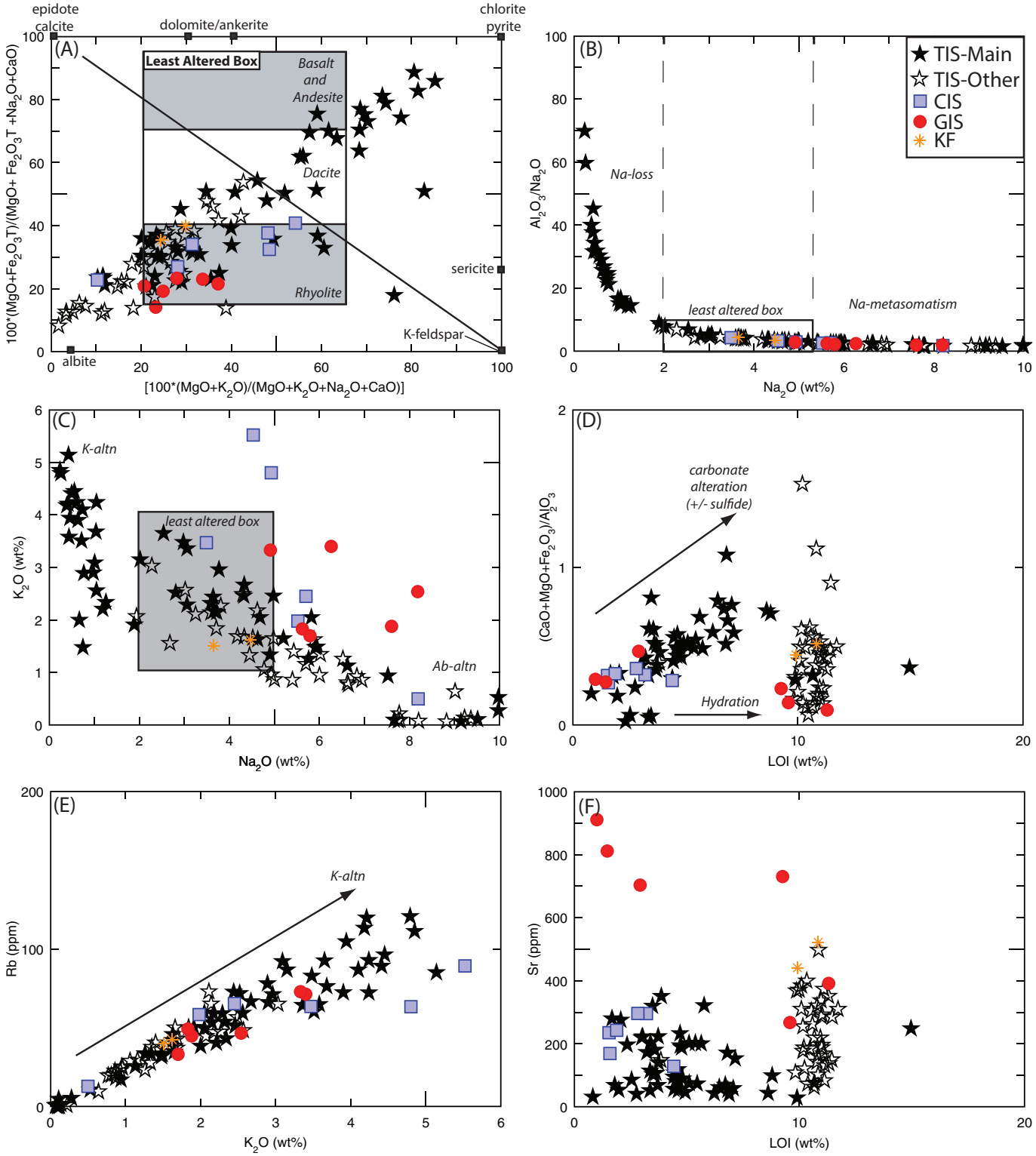

Fig. 7. Isocon plots (Grant 1986) of least altered porphyry sample against various "type" alteration associated with the porphyry intrusive rocks and volcanic rocks. Notably, in all cases the high field strength elements (HFSE) and Al_2O_3 are immobile, therefore illustrating that they are seeing through hydrothermal alteration. A similar case exists for the rare earth elements (REE) and TiO_2, except for minor mobility in the intensely carbonate altered samples. Nevertheless, even in the carbonate alteration there are constant inter-REE ratios, suggesting that they still can be used for primary petrological–chemostratigraphic information. Isocon scaling factors were obtained using the modified isocon method of Huston (1993) and are unique for each sample. LFSE, low field strength elements, TIS, Timmins porphyry intrusive suite (main camp and other); CIS, Carr Township porphyry intrusive suite; GIS, granodiorite intrusive suite; and KF, Krist Formation. [Colour online.]

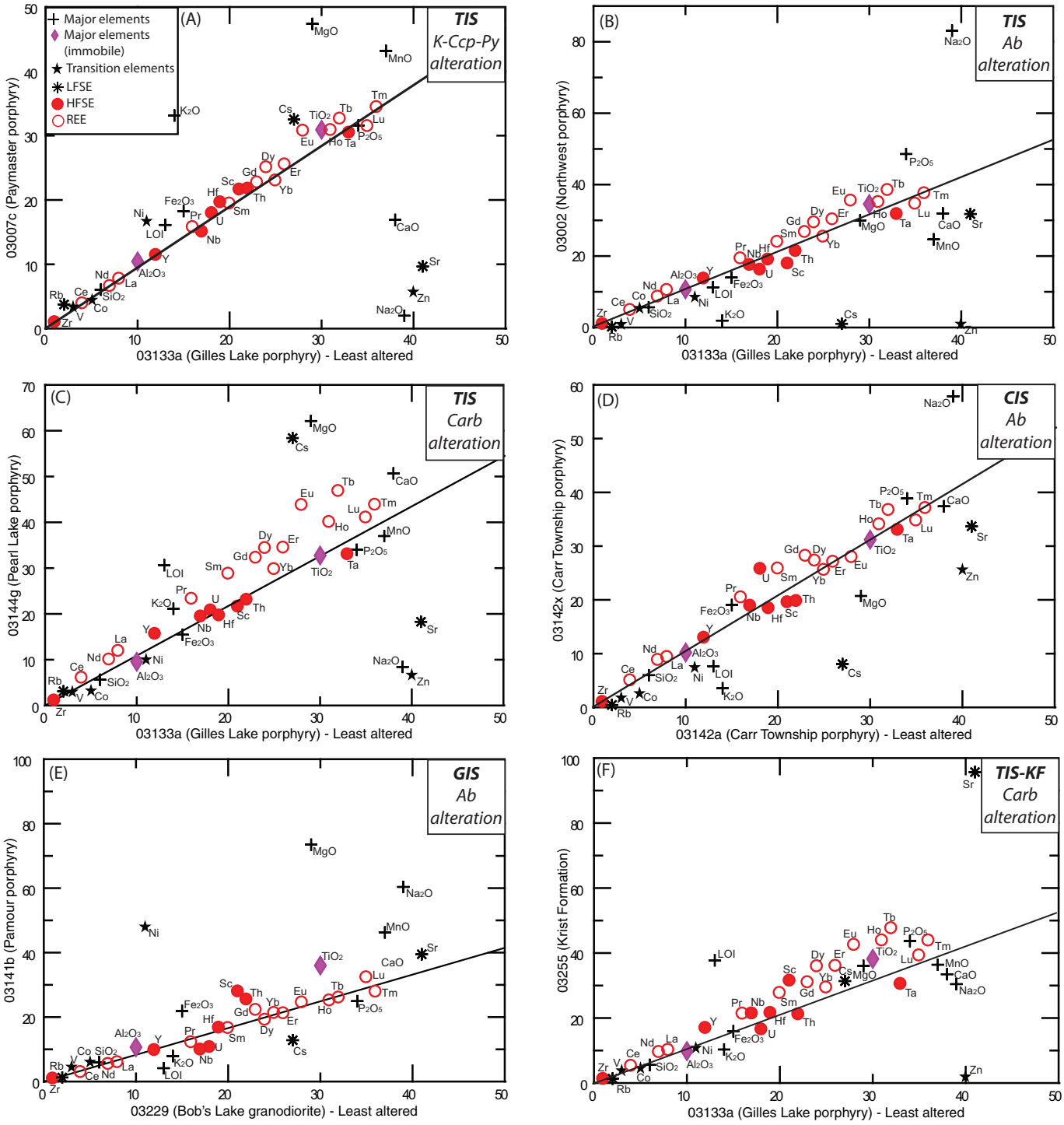

similar to other Archean TTG suites and have adakite-like affinities (Fig. 9D). Primitive mantle-normalized multi-element plots for the TIS are characterized by steep patterns with light REE (LREE)-enrichment and heavy-REE (HREE) depletion coupled with negative Nb and Ti anomalies and positive Zr, Hf, and Al anomalies (Figs. 10A–10B). This suite also has M-type Nb-Y ratios and Sc/Y = ~0.5–1.0 that are consistent with generation at depths in the garnet–hornblende stability field (Fig. 11).

Fig. 8. Immobile element discrimination plots for the Porcupine intrusive suites and the Krist Formation, including: (A) Y versus Nb, (B) Zr versus TiO_2, (C) Nb versus Zr, and (D) Yb versus Th. All values are given in parts per million, except for TiO_2, which is given in weight percent. TIS, Timmins porphyry intrusive suite (main camp and other); CIS, Carr Township porphyry intrusive suite; GIS, granodiorite intrusive suite; and KF, Krist Formation. [Colour online.]

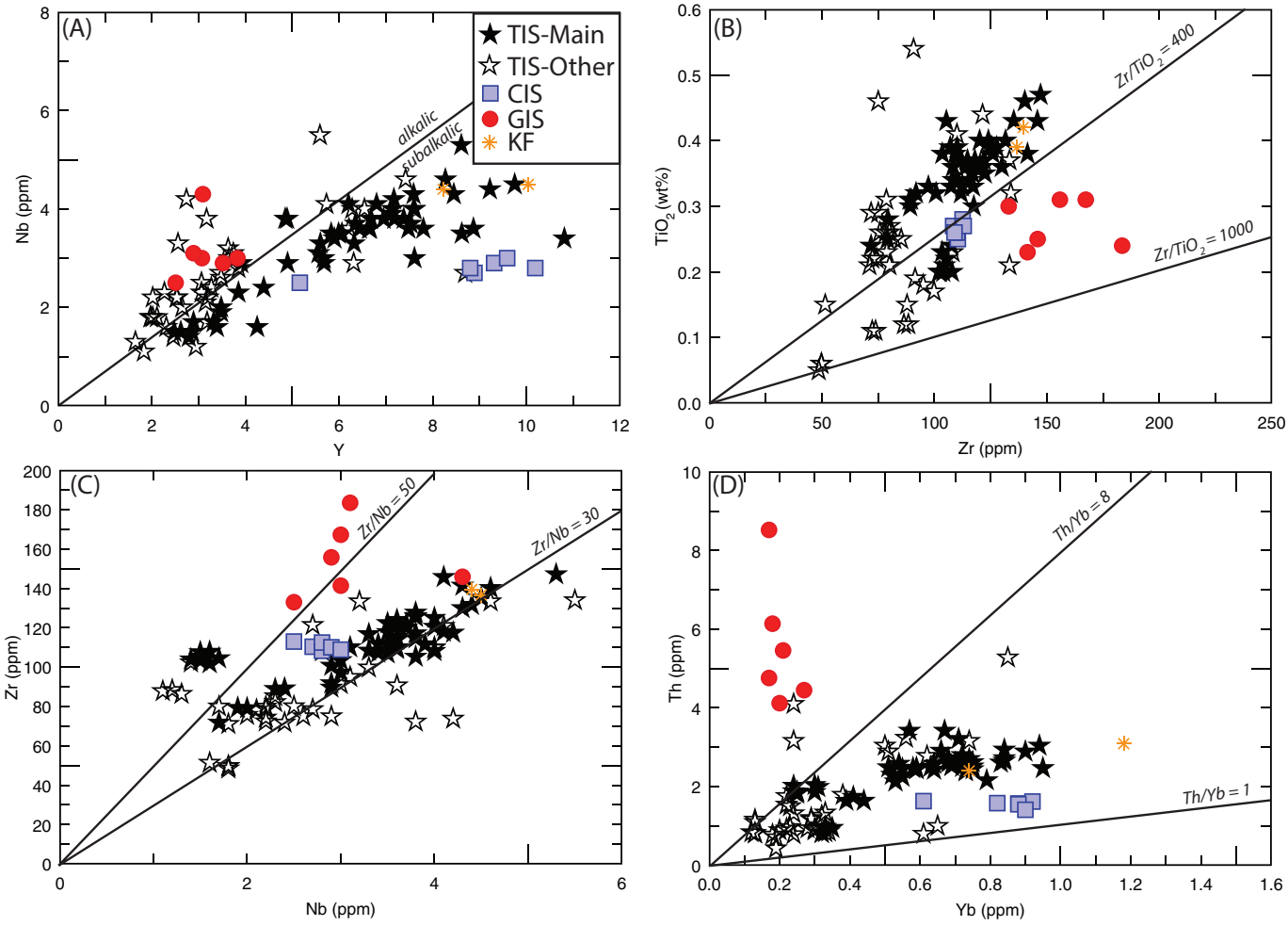

CIS

The CIS has subalkalic affinities with Nb/Y<0.7, andesitic to dacitic Zr/TiO_2, and calc-alkalic affinities with Zr/Y>4.5, Zr/Nb ~30–50, and Th/Yb>0.85 (Figs. 8 and 9) (e.g., Barrett and MacLean 1994; Barrett and MacLean 1999). The CIS has high-Al TTG affinities like the TIS, but it has lower La/Yb ratios and higher Yb concentrations (Fig. 9). The lower La/Yb is echoed in the primitive mantle normalized plots in which the CIS have similar patterns to the TIS, but with lesser LREE-enrichment and HREE depletion; they have similar negative anomalies at Nb, Ti, and low V-Sc and positive Zr–Hf–Al anomalies (Fig. 10). The CIS has M-type affinities with low Nb and Y contents, and Sc/Y~0.3–0.7, consistent with hornblende being present in the residue during crustal partial melting (Fig. 11).

GIS

The GIS is somewhat different than the other suites in that the entire population has alkalic affinities with Nb/Y>0.7 and very high Zr/Y, Zr/Nb, Th/Yb, and La/Yb relative to the TIS and CIS (Figs. 8–9). The Zr/Y and Th/Yb affinities of the GIS are consistent with a calc-alkalic affinity and their relatively low Yb but variable Al_2O_3 contents give them low- to high-Al TTG affinities (Fig. 9). The GIS have very high La/Yb (Fig. 9D) and extremely steep primitive mantle normalized patterns with significant depletions in HREE, enrichments in LREE, and negative Nb and Ti anomalies (Fig. 10D). Like the TIS and the CIS, the GIS has M-type Nb–Y systematics and Sc/Y ~0.5 consistent with garnet–hornblende in the residue during crustal partial melting (Fig. 11).

KF

The KF is subalkaline and has calc-alkalic to alkalic signatures (Figs. 8–9) that lie close to the low-Al TTG-high-Al TTG boundary with adakite-like La/Yb–Yb systematics (Fig. 9). Their primitive mantle normalized signatures are similar to the TIS and CIS, with LREE enrichment, HREE depletion, and variably developed negative Nb–Ti and positive Zr–Hf–Al anomalies (Fig. 10E). The KF has M-type affinities and Sc/Y ~0.5–1 consistent with garnet–hornblende in the residues during partial melting (Fig. 11).

Discussion

Petrogenesis of the Porcupine intrusive suites

All of the Porcupine intrusive suites have broadly similar geochemical signatures with small, yet significant, differences that indicate potentially distinct petrogenetic histories. The TIS, GIS, and KF, have high-Al TTG lithogeochemical affinities with adakite-like signatures of HREE depletion (Figs. 8–11). Two main models have been proposed to explain the genesis of TTG suites in modern and ancient settings: (*i*) slab-melting of subducted oceanic crust and (or) (*ii*) the delamination and hydrous melting of

Fig. 9. Classification plots for adakite-like rocks for the Porcupine intrusive suites and the Krist Formation, including: (A) Nb/Y versus Zr/TiO_2 discrimination diagram of Winchester and Floyd (1977; modified by Pearce 1996); (B) Y versus Zr diagram from Ross and Bedard (2009); (C) Al_2O_3 versus Yb diagram of Arth (1979) classifying different types of tonalite–trondhjemite–granodiorite (TTG); (D) Yb versus La/Yb (modified from Castillo et al. 1999). Adakite field from Defant and Drummond (1990). All values are given in parts per million, except for Al_2O_3 and TiO_2, which are given in weight percent. TIS, Timmins porphyry intrusive suite (main camp and other); CIS, Carr Township porphyry intrusive suite; GIS, granodiorite intrusive suite; and KF, Krist Formation. [Colour online.]

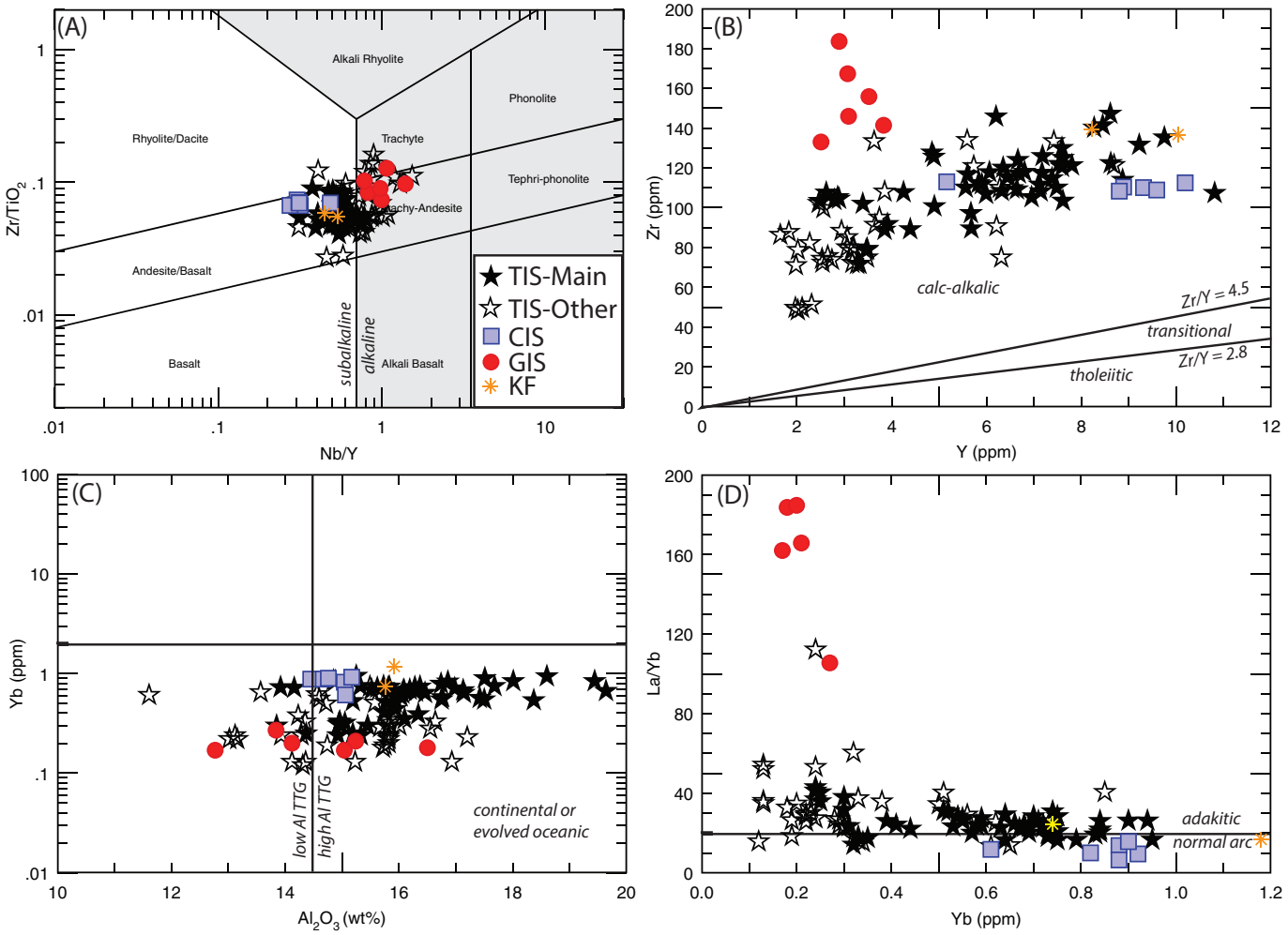

stacked and thickened mafic crust (Drummond and Defant 1990; Drummond et al. 1996; Martin 1999; Martin and Moyen 2002; Martin et al. 2005; Bedard 2006; Jiang et al. 2007; Wang et al. 2007; Smithies 2000; Piercey et al. 2008; Wyman and Kerrich 2009; Moyen 2009). In the case of the slab melt model, workers have suggested that slab-melts would have reacted with the mantle wedge resulting in TTG-like rocks with enrichments in MgO, Cr, and Ni (e.g., Defant and Drummond 1990; Martin et al. 2005; Rapp et al. 1999; Bedard 2006; Richards and Kerrich 2007). The absence of MgO, Cr, and Ni enrichments in the TIS argue against slab melt – mantle wedge interactions and a slab melt model for their origin (e.g., Martin et al. 2005; Rapp et al. 1999; Bedard 2006; Richards and Kerrich 2007). In contrast, the melting of mafic crust related to delamination of stacked and thickened basaltic crust, with garnet and hornblende stable in the restite, best explains the geochemistry of the TIS suite (e.g., Rapp et al. 1991; Feng and Kerrich 1992; Wyllie et al. 1997; Rapp 1997; Moyen and Stevens 2006; Piercey et al. 2008; Beakhouse 2011). This is also consistent with the geological evolution of the Timmins region. For example, the TIS suite porphyries postdate early extension and pretectonic magmatism (e.g., Beakhouse 2011; Bleeker 2015) and are considered early syntectonic and coincident with ~2690 Ma D1 uplift and crustal thickening (Fig. 12) (Bateman et al. 2008; Dubé et al. 2017). Crustal thickening, coupled with possible delamination (e.g., Bedard 2006), is a possible mechanism that would result in crustal melting at elevated pressures where garnet and hornblende would be stable in the restite and results in the generation of the high-Al TTG signatures in the TIS (Beakhouse 2011; Bleeker 2015).

The CIS has high-Al TTG and adakite affinities, like the TIS, but differs in having granitic to trondhjemitic compositions, lower Sc/Y, La/Yb, and less depletion in HREE. This suggests that they formed via partial melting of mafic crust but at shallower crustal levels than the TIS, where garnet was not a stable phase in the melt residue (e.g., Rapp et al. 1991; Feng and Kerrich 1992; Wyllie et al. 1997; Rapp 1997; Moyen and Stevens 2006; Piercey et al. 2008). The timing of CIS TTG genesis is post-D2 crustal thickening (~2690–2680 Ma: Fig. 12) and coincides with post-D2 regional extension (~2685–2670 Ma: Fig. 12) (Bateman et al. 2008); these plutons are likely similar to the post-tectonic to late-tectonic suite of Beakhouse (2011). Further, it is possible that the initial D1 crustal thickening produced sufficient heat to induce mafic crustal melting at shallower crustal levels when compared with the TIS and,

Fig. 10. Primitive mantle normalized multi-element plots, with inset chondrite normalized rare earth element plots, for the Porcupine intrusive suites and the Krist Formation, including: (A) Timmins porphyry intrusive suite (TIS-main camp), (B) Timmins porphyry intrusive suite (TIS-other), (C) Carr Township porphyry intrusive suite (CIS), (D) granodiorite intrusive suite (GIS), and (E) Krist Formation (KF). Primitive mantle values from Sun and McDonough (1989). [Colour online.]

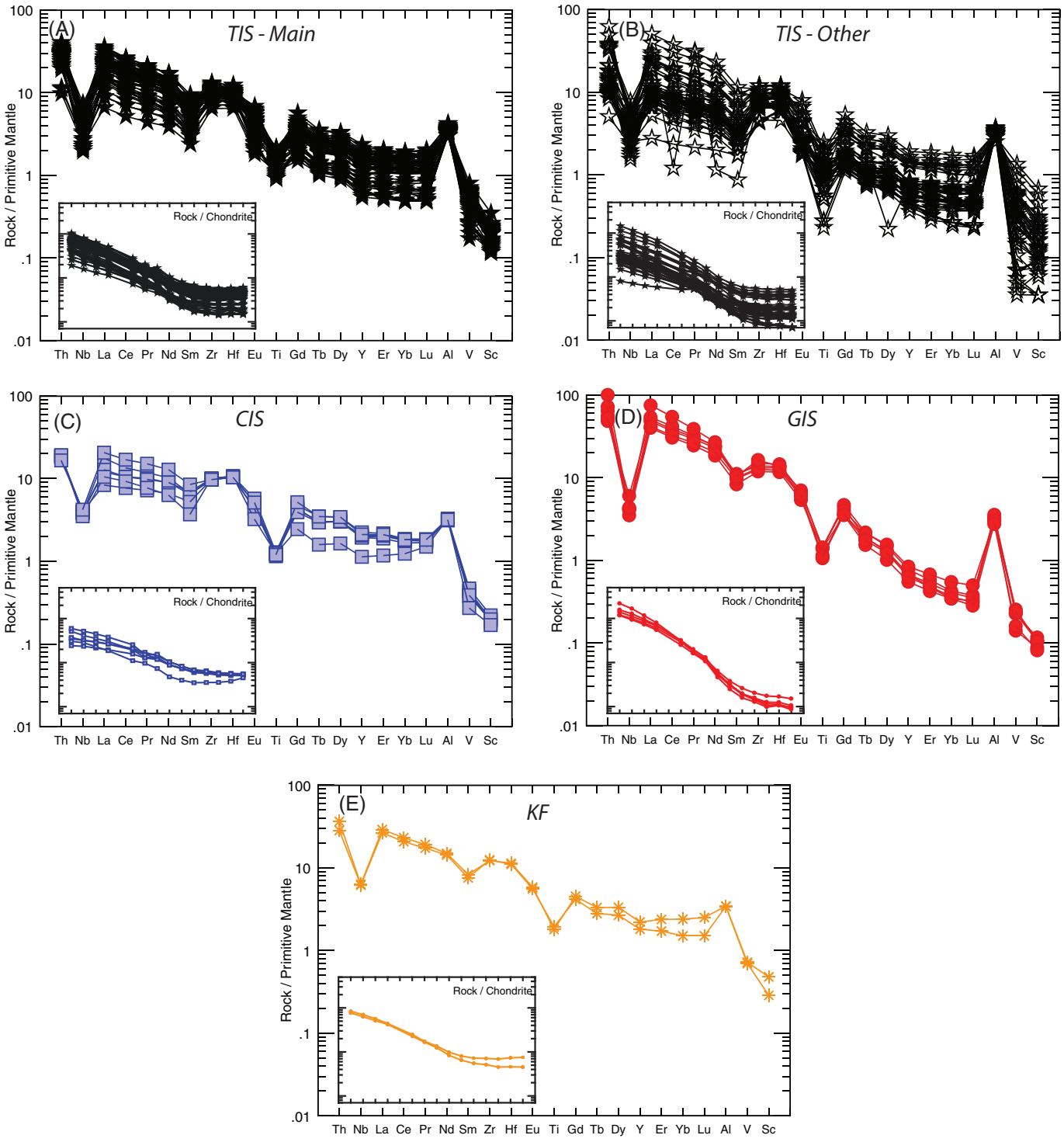

coupled with extensional activity, permitted emplacement of the CIS into upper crustal levels.

The GIS has steeper REE patterns and more fractionated HREE compared with the TIS and CIS consistent with derivation at greater depths and pressures than the TIS and CIS where there was likely more garnet in the melt residue (e.g., Rapp et al. 1991; Feng and Kerrich 1992; Wyllie et al. 1997; Rapp 1997; Moyen and Stevens 2006; Piercey et al. 2008). This suite of magmas formed via partial melting of a mafic source, similar to the TIS and CIS, but it was during crustal thickening during or after D2 thrust faulting (Fig. 12) (i.e., syntectonic; Bateman et al. 2008; Beakhouse 2011).

In summary, the Porcupine intrusive suites are predominantly related to lower crustal melting of mafic crust at varying pressures where there were varying abundances of garnet and hornblende

Fig. 11. Discrimination plots for the Porcupine intrusive suites and the Krist Formation, including: (A) Y versus Nb diagram from Pearce et al. (1984) and (B) Y versus Sc plot from Feng and Kerrich (1992). All values are given in parts per million. TIS, Timmins porphyry intrusive suite (main camp and other); CIS, Carr Township porphyry intrusive suite; GIS, granodiorite intrusive suite; and KF, Krist Formation. [Colour online.]

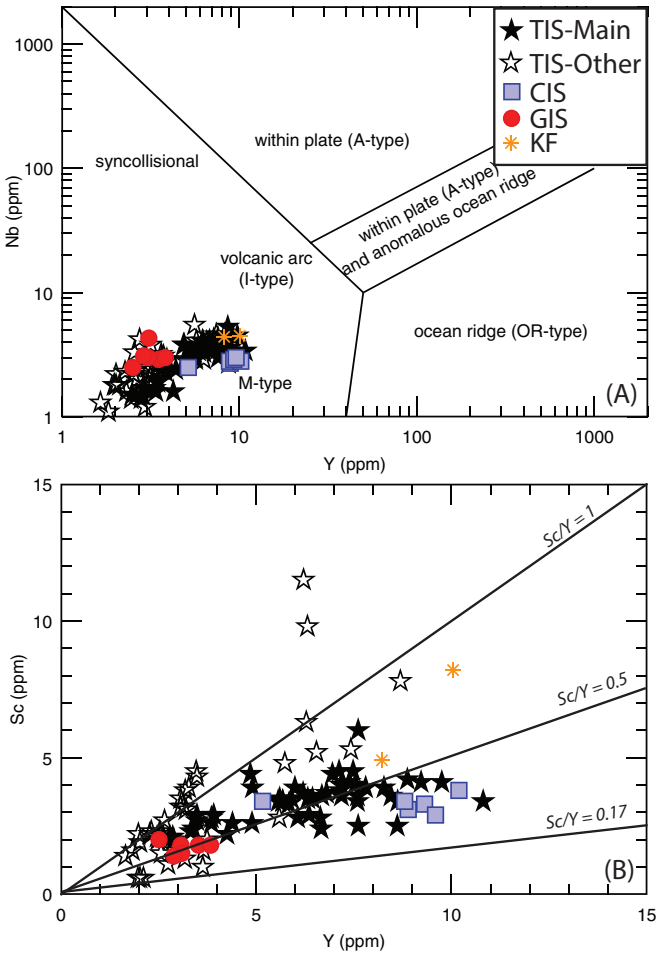

in the melt residue (e.g., Wylie et al. 1997). Although this could be related to different source rocks, the spatial proximity of the different suites and established architecture of the Timmins area (Ayer et al. 2002; Bateman et al. 2008; Thurston et al. 2008; Bleeker 2015; Dubé et al. 2017), suggests that their petrogenetic differences were likely related to depth of partial melting rather than differences in source rock. Furthermore, based on REE–HFSE systematics, it is interpreted that the CIS was derived at the shallowest crustal levels, whereas TIS and GIS were formed at greater depths, respectively. The Porcupine intrusive suites also span the entire early deformational history of the Timmins–Porcupine gold camp with the TIS forming coeval with D1 (early syntectonic) and the CIS and GIS forming post-D2/pre-D3 (syntectonic to late syntectonic) (Fig. 12).

Relationship of KF volcanism to the emplacement of the Porcupine intrusive suites

The KF has geographic distribution, petrographic characteristics, and U–Pb ages that are very similar to the TIS (Ayer et al. 2003*b*), as well as similar lithogeochemical signatures. These similarities suggest that the TIS and KF are coeval and potentially share a similar petrogenetic history. While there are no direct physical linkages between the TIS and KF, there is field evidence that suggests that despite the melts for the TIS being generated at depth, the TIS was emplaced at shallow crustal levels in a subvolcanic environment (<1 km from surface?). For example, the very fine-grained matrix of the TIS implies quick cooling as subvolcanic intrusions in the near surface (e.g., Mason and Melnik 1986). Shallow emplacement of the TIS is further supported by flow-banded breccias in the Paymaster porphyry near the Dome mine, which suggest that it may have been emplaced as subvolcanic cryptodomes (Pyke 1982; Cas et al. 1990). These data suggest that the TIS intrusions are most likely the subvolcanic roots of the extrusive KF.

Discriminating gold-bearing and gold-barren intrusions in the Timmins–Porcupine gold camp

All Porcupine intrusive suites display a spatial association with gold mineralization; however, there are systematic lithogeochemical differences and specific suites associated with the largest gold deposits. For example, the largest gold deposits in the Timmins–Porcupine gold camp (i.e., >10 MOz of Au produced), including the Hollinger, McIntyre, and Dome mines, are spatially associated with the TIS (Brisbin 2000). Similarly, moderate-sized gold deposits (production or indicated Au reserves ≥1 MOz), including the Coniaurium, Preston, Paymaster, Buffalo Ankerite, Hoyle Pond, and Aquarius mines, and small gold deposits (production or indicated Au reserves <1 million ounces), including the Vipond, Moneta, Crown, Gillies Lake, and Fuller (Vedron) mines, are also associated with TIS (Brisbin 2000) (e.g., Fig. 2). The exception includes the small Naybob mine (50 733 ounces of Au produced), which is associated with the GIS (Brisbin 2000). The only intrusions in the TIS not spatially associated with gold are located south of the PDDZ. Furthermore, the GIS (excluding the aforementioned Naybob porphyry) and CIS are not associated with significant gold accumulations. This suggests that TIS intrusions north of the PDDZ are the most prospective suite of the Porcupine intrusive rocks (Fig. 1).

Alteration geochemistry is also useful in distinguishing potentially gold mineralized versus barren intrusions. Samples associated with the large gold deposits preferentially plot to the right side of the alteration box plot (Fig. 6A), have evidence K-metasomatism, show strong Na_2O and Sr depletions, and have elevated Al_2O_3/Na_2O, K_2O, K_2O/Na_2O, Rb, and Cs (Figs. 6 and 7; Suppplementary Table1[1]). In contrast, intrusions related to moderate sized deposits preferentially plot in the least altered fields or have experienced Na-metasomatism and carbonate alteration only (Fig. 6). Furthermore, intrusions associated with small gold deposits and barren intrusions preferentially plot in the least altered field with some samples exhibiting weak Na-alteration (Figs. 6A–6C). Similarly, alteration mineralogy correlates with alteration geochemical signatures. Large deposits have intrusions with significant sulfide alteration (pyrite ± pyrrhotite ± chalcopyrite) and sericite-calcium carbonate alteration (Table 1). Moderate sized deposits have weak to moderate albite + Fe-carbonate alteration (Table 1). Small gold occurrences are associated with associated intrusions that are unaltered to weakly albite altered (Table 1).

Alteration geochemistry, in combination with petrography, suggests that large gold deposits (>10 million ounces) in the Timmins–Porcupine gold camp are associated with structurally controlled intense K-metasomatism and associated sericite alteration. These large deposits are surrounded by moderate-sized gold deposits (≥1 million ounces), often hosted within the same structures (e.g., Hollinger shear zone and Dome fault), but associated with weaker K-metasomatism–sericite alteration and increased Na-metasomatism–albite + Fe-carbonate alteration. Small gold deposits (<1 million ounces) are also present along the same structures that host large deposits, but are associated with intrusions that display weak Na-metasomatism–albite alteration.

Fig. 12. Chronology of volcanism, sedimentation, intrusive magmatism, deformation, metamorphism, and mineralization in the Timmins–Porcupine gold camp. Modified from Bateman et al. (2005). TIS, Timmins porphyry intrusive suite (main camp and other); CIS, Carr Township porphyry intrusive suite; and GIS, granodiorite intrusive suite. [Colour online.]

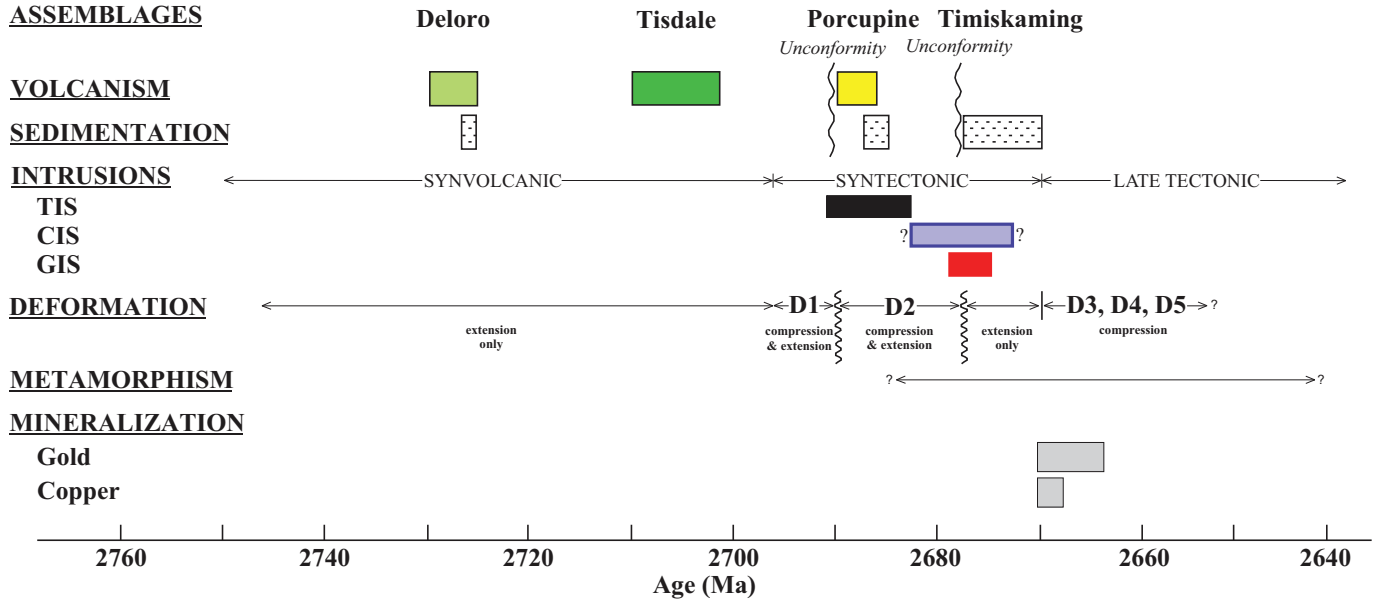

Deciphering the relationship between the Porcupine intrusive suites and gold mineralization

The relationship of gold mineralization to porphyries has been an important question within the Timmins–Porcupine gold camp as numerous deposits occur proximal to Porcupine intrusive suite rocks (see Fig. 2). Some previous workers have suggested a genetic link between the Porcupine intrusive suite magmatic–hydrothermal processes and gold mineralization (e.g., Davies and Luhta 1978; Mason 1986*a*, 1986*b*; Mason and Melnik 1986; Brisbin 2000; Gray and Hutchinson 2001), whereas others have suggested that there is a structural relationship (e.g., Burrows et al. 1993; Dubé et al. 2017).

The results of this study, and other studies (e.g., Burrows et al. 1993), indicate that there is no significant evidence for a magmatic–hydrothermal association between the porphyry intrusions and gold mineralization. Numerous arguments support this assertion. First, much of the gold mined within the Timmins–Porcupine gold camp does not occur in the intrusions but along their margins in Fe-rich mafic volcanic wall rocks (e.g., Melnik-Proud 1992; Brisbin 2000; Gray and Hutchinson 2001). In the cases where gold is present and mined within the intrusions, the majority of veins originate and are centered in volcanic rocks peripheral to the intrusions within favorable structural traps (Burrows et al. 1993; Dubé et al. 2017). Second, most of the ore veins mined in the camp crosscut a younger intrusive suite (albitite dikes), which themselves crosscut the Porcupine intrusive suite suggesting a temporal gap between Porcupine intrusive suite magmatism and gold mineralization (Mason 1986a; Mason and Melnik 1986; Brisbin 2000). Third, Re-Os dating of molybdenite from both the McIntyre and Dome mines yielded ages of 2670–2672 Ma (Bateman et al. 2004; Ayer et al. 2003*b*, 2005), which are at least 15 million years younger than the emplacement of the Porcupine intrusive suites (2677–2691 Ma) (Corfu et al. 1989; Gray and Hutchinson 2001; Ayer et al. 2002, 2003*b*; MacDonald et al. 2005). Finally, arguments presented within illustrate the TIS intrusions are pre- to syn-D2, whereas gold mineralization has been shown to be associated with a regional D3 shortening episode (i.e., younger than the porphyries of this study), implying the porphyries were present prior to Au-emplacement during regional D3 deformation (Dubé et al. 2017).

While no genetic magmatic–hydrothermal relationship exists between gold mineralization and the Porcupine intrusive suites, there is a strong spatial association between porphyries and gold mineralization. Two models have been proposed to explain this relationship. The first suggests that Porcupine intrusive suite and subsequent gold systems utilized the same, protracted and (or) reactivated structural conduits for their emplacement (Brisbin 2000). This is supported by the spatial association of both intrusions and major gold deposits along the same structures, including the Hollinger high strain zone, the Dome fault, and the PDDZ (Fig. 1) (Brisbin 2000). In this model the regional deformation zones that facilitated porphyry intrusion emplacement were reactivated during the main gold-forming events (Ayer et al. 2003*b*; Corfu et al. 1989; Bateman et al. 2004; Bleeker 2015).

Alternatively, and potentially coincidental, the competency contrast between competent Porcupine intrusive suite and less competent mafic volcanic country rocks could have acted as a locus for deformation (Gorman et al. 1981; Burrows et al. 1993; Burrows and Spooner 1989; Wood et al. 1986; Dubé et al. 2017). The intrusions may have acted like "pillars" (Wood et al. 1986) within the mafic volcanic rocks and deflected deformation resulting in high strain and dilational zones around the margins of the intrusions into which the Au-bearing fluids migrated (Burrows et al. 1993; Burrows and Spooner 1989; Wood et al. 1986). The reaction of the Au-bearing fluid with Fe-rich Tisdale Assemblage volcanic rocks along porphyry-Tisdale Assemblage contact dilation zones likely resulted in the destabilization of Au thiocomplexes, due to wall rock sulphidation, resulting in Au to be precipitated from solution (e.g., Seward 1973; Ropchan et al. 2002; Dinel et al. 2008; Dubé et al. 2017). Key support for this hypothesis is that the majority of the gold was mined outside of the intrusions along the margins of the intrusive bodies within associated marginal high strain zones and volcanic rocks of the Tisdale Assemblage (e.g., Hollinger–McIntyre and Dome) (Mason and Melnik, 1986; Mason 1986*a*; Burrows et al. 1993; Brisbin 2000; Gray and Hutchinson 2001; Bateman et al. 2008).

Given the above relationships we suggest a hybrid model where porphyry intrusions were emplaced along regional faults, and during subsequent regional deformation, the location and competency contrasts between porphyry intrusions and their wall

rocks caused the reactivation of these structures creating dilational zones surrounding the porphyries that were favorable for ore fluid migration and gold precipitation. It is also notable that larger gold deposits within the Timmins–Porcupine camp (e.g., Hollinger, McIntyre, and Dome mines) are located where there are multiple, coalesced intrusions (e.g., Preston and Paymaster porphyries at Dome), and intrusion coalescence likely caused larger dilation zones during deformation, better structural traps, and increased the potential to form larger gold deposits. This coalescing of intrusive rocks near major structures may be a potential tool for further exploration in both the Timmins–Porcupine camp and other similar gold camps globally.

Conclusions

There are at least three distinct petrogenetic suites of porphyry intrusions along the PDDZ in the Timmins–Porcupine gold camp. The majority of the intrusions are related to magma generated via crustal thickening at ca. 2690 Ma during D1 deformation. Despite formation at depth with garnet and hornblende in the residue, the TIS magmas were emplaced at shallow depths and represent subvolcanic intrusions to the eruptive pyroclastic rocks of the KF. Approximately 10–15 million years after the TIS–KF magmatic event, two other magma suites were generated from melting of mafic lower crustal rocks. The CIS was generated by crustal melting at shallower crustal depths than the TIS (i.e., hornblende in the residue), whereas the GIS was generated at greater depths (i.e., garnet–hornblende in the residue) than the TIS. The temporal gap between the TIS and GIS, the interpreted progressive depth of melting, and that the two intrusive suites have intruded within the immediate vicinity of one another, suggests that D2 thrust stacking in the Timmins area significantly thickened the crust between 2690–2678 Ma causing deeper magma generation.

Gold mineralization is associated with all of the Porcupine intrusive suites. However, large gold deposits (>10 million ounces) are only related to the TIS intrusions that have strong pyrite and potassic alteration. Moderate-sized gold deposits (>1 million ounces) are also predominantly associated with the TIS, but have weak to moderate sodic and carbonate alteration. Small gold deposits (<1 million ounces) and anomalous gold showings are associated with only weak sodic alteration and are predominantly proximal to TIS and to a lesser extent the GIS intrusions. Barren intrusions include the TIS intrusions south of the PDDZ and the CIS and GIS intrusions east of the Burrows–Benedict Fault.

Porphyries that lie along a similar structure in the Timmins region can be associated with large gold systems that contain cores of strong potassic alteration and are often spatially proximal to smaller gold deposits where the porphyries contain weak sodic alteration. This alteration pattern is similar to those developed around Phanerozoic porphyry systems; however, regional and local geological arguments and geochronology argue that gold mineralization does not have a magmatic–hydrothermal relationship with the Porcupine intrusive suites. Instead, the spatial association is related to the Porcupine intrusive suites and Au-mineralizing fluids utilizing the same structural conduits. It is suggested that reactivation of regional faults and the creation of hydrodynamically favourable dilation zones along the margins of intrusions and their contacts with Fe-rich rocks of the Tisdale Assemblage allowed Au-bearing fluids to migrate peripheral to the intrusions, undergo wall rock sulphidation, and form gold mineralization. This coincidence of structural and chemical traps along porphyrie margins was critical in forming the world-class mineralization found in the Timmins–Porcupine gold camp.

Acknowledgements

This paper constitutes part of the senior author's M.Sc. thesis at Laurentian University and was supported by the Discover Abitibi Initiative and a Discovery Grant to Piercey from the Natural Sciences and Engineering Research Council of Canada (NSERC). During final completion of this manuscript Piercey was funded by the NSERC-Altius Industrial Research Chair at Memorial University funded by NSERC, Altius Resources Inc., and the Research and Development Corporation of Newfoundland and Labrador. Phil Thurston and John Ayer are thanked for their administrative and scientific contributions to this Discover Abitibi Project and the research that was undertaken in this manuscript. Reviews of previous drafts of this manuscript by John Ayer, Gary Beakhouse, Phil Thurston, Bruno Lafrance, Dan Kontak, Ben Berger, and David John are greatly appreciated. Constructive reviews by three anonymous *CJES* reviewers are also acknowledged for helping improve this manuscript. Final thanks to the many geologists who worked in the Timmins camp and freely shared their knowledge with us; they helped shape our understanding of the Timmins camp.

References

Ahmed, A.D., Hood, S.B., Gazley, M.F., Cooke, D.R., and Orovan, E.A. 2019. Interpreting element addition and depletion at the Ann Mason porphyry-Cu deposit, Nevada, using mapped mass balance patterns. Journal of Geochemical Exploration, **196**: 81–94. doi:10.1016/j.gexplo.2018.09.009.

Arth, J.G. 1979. Some trace elements in trondhjemites - their implications to magma genesis and paleotectonic setting. *In* Trondhjemites, dacites, and related rocks. *Edited by* F. Barker. Elsevier Scientific Publishing Co., pp. 123–132.

Ayer, J.A., Berger, B.R., and Trowell, N.F. 1999*a*. Geological Compilation of the Lake Abitibi area, Abitibi greenstone belt, Map P.3398, 1:100,000 scale. Ontario Geological Survey.

Ayer, J.A., Berger, B.R., and Trowell, N.F. 1999*b*. Geological Compilation of the Timmins area, Abitibi greenstone belt, Map P.3398, 1:100,000 scale. Ontario Geological Survey, **1**:100000.

Ayer, J., Amelin, Y., Corfu, F., Kamo, S., Ketchum, J.F., Kwok, K., and Trowell, N.F. 2002. Evolution of the Abitibi greenstone belt based on U-Pb geochronology: autochthonous volcanic construction followed by plutonism, regional deformation and sedimentation. Precambrian Research, **115**: 63–95. doi:10.1016/S0301-9268(02)00006-2.

Ayer, J., Thurston, P.C., Dubé, B., Fowler, A.D., Gibson, H.L., Hudak, G.J., Lafrance, B., Lesher, C.M., Piercey, S.J., Reed, L.E., and Thompson, P.H. 2003*a*. Overview of the Discover Abitibi Greenstone Architecture Project: subprojects, goals and results. *In* Summary of field work and other activities 2003. Ontario Geological Survey, Open File Report 6120, pp. 32-1 to 32-12.

Ayer, J.A., Barr, E., Bleeker, W., Creaser, R.A., Hall, G., Ketchum, J.W.F., Powers, D., Salier, B., Still, A., and Trowell, N.F. 2003*b*. 33. Discover Abitibi. New geochronological results from the Timmins area: implications for the timing of late-tectonic stratigraphy, magmatism and gold mineralization. *In* Summary of field work and other activities 2003. Ontario Geological Survey, Open File Report 6120, pp. 33.1–33.11.

Ayer, J.A., Thurston, P.C., Bateman, R., Dubé, B., Gibson, H.L., Hamilton, M.A., Hathway, B., Hocker, S.M., Houlé, M., Hudak, G., Lafrance, B., Lesher, C.M., Isopolatov, V., MacDonald, P.J., Péloquin, A.S., Piercey, S.J., Reed, L.H., and Thompson, P.H. 2005. Overview of results from the Greenstone Architecture Project: Discover Abitibi Initiative. Ontario Geological Survey Open File 6154, 146 p.

Barrett, T.J., and MacLean, W.H. 1994. Chemostratigraphy and hydrothermal alteration in exploration for VHMS deposits in greenstones and younger rocks. *In* Alteration and alteration processes associated with ore-forming systems. *Edited by* D.R. Lentz. Geological Association of Canada, Short Course Notes Vol. 11, pp. 433–467.

Barrett, T.J., and MacLean, W.H. 1999. Volcanic sequences, lithogeochemistry, and hydrothermal alteration in some bimodal volcanic-associated massive sulfide systems. Reviews in Economic Geology, **8**: 101–131. doi:10.5382/Rev.08.05.

Bateman, R., Ayer, J.A., Barr, E., Dubé, B., and Hamilton, M.A. 2004. Discover Abitibi, Gold Subproject 1; protracted structural evolution of the Timmins-Porcupine gold camp and the Porcupine-Destor deformation zone. *In* Summary of field work and other activities 2004. Ontario Geological Survey, Open File 6145, pp. 41.1–41.10.

Bateman, R., Ayer, J.A., Dubé, B., and Hamilton, M.A. 2005. The Timmins-Porcupine gold camp, northern Ontario; the anatomy of an Archaean greenstone belt and its gold mineralization; Discover Abitibi Initiative. Ontario Geological Survey: Sudbury, Ont. Open File 6158, 90 p.

Bateman, R., Ayer, J.A., and Dubé, B. 2008. The Timmins-Porcupine Gold Camp, Ontario: anatomy of an Archean greenstone belt and ontogeny of gold mineralization. Economic Geology, **103**: 1285–1308. doi:10.2113/gsecongeo.103.6.1285.

Beakhouse, G.P. 2011. The Abitibi Subprovince plutonic record: tectonic and metallogenic implications. Ontario Geological Survey, Open File Report **6268**, 161p.

Bedard, J.H. 2006. A catalytic delamination-driven model for coupled genesis of

Archaean crust and sub-continental lithospheric mantle. Geochimica et Cosmochimica Acta, **70**: 1188–1214. doi:10.1016/j.gca.2005.11.008.

Bleeker, W. 2015. Synorogenic gold mineralization in granite-greenstone terranes: the deep connection between extension, major faults, synorogenic clastic basins, magmatism, thrust inversion, and long-term preservation. *In* Targeted Geoscience Initiative 4: Contributions to the Understanding of Precambrian Lode Gold Deposits and Implications for Exploration. *Edited by* B. Dubé and P. Mercier-Langevin. Geological Survey of Canada, Open File 7852, pp. 25–47.

Brisbin, D.I. 1997. Geological setting of gold deposits in the Porcupine mining district, Timmins, Ontario. Unpublished Ph.D. thesis, Queen's University, 523 p.

Brisbin, D.I. 2000. World class intrusion-related Archean vein gold deposits of the Porcupine gold camp, Timmins, Ontario. *In* Geology and Ore Deposits 2000: The Great tk;4Basin and Beyond Symposium Proceedings. *Edited by* J.K. Cluer et al. Geological Society of Nevada, pp. 19–35.

Burnham, O.M., and Schweyer, J. 2004. 54. Trace element analysis of geological samples by inductively coupled plasma mass spectrometry at the Geoscience Laboratories: revised capabilities due to improvements to instrumentation. *In* Summary of fieldwork and other activities 2004. Ontario Geological Survey, Open File 6145, pp. 54.1–54.20.

Burnham, O.M., Hechler, J., Semenyna, L., and Schweyer, J. 2002. Mineralogical controls on the determination of trace elements following mixed-acid dissolution. Ontario Geological Survey, Open File Report 6100, 36.1–12 p.

Burrows, A.G. 1925. The Porcupine gold area. Ontario Bureau of Mines, 112 p.

Burrows, D.R., and Spooner, E.T.C. 1986. The McIntyre Cu-Au deposit, Timmins, Ontario, Canada. *In* Proceedings of Gold '86: An International Symposium on the Geology of Gold Deposits. *Edited by* A.J. MacDonald. pp. 23–39.

Burrows, D.R., and Spooner, E.T.C. 1989. Relationships between Archean gold quartz vein-shear zone mineralization and igneous intrusions in the Val d'Or and Timmins areas, Abitibi Subprovince, Canada. Economic Geology Monographs, **6**: 424–444. doi:10.5382/Mono.06.33.

Burrows, D.R., Spooner, E.T.C., Wood, P.C., and Jemielita, R.A. 1993. Structural controls on formation of the Hollinger-McIntyre Au quartz vein system in the Hollinger shear zone, Timmins, southern Abitibi greenstone belt, Ontario. Economic Geology, **88**: 1643–1663. doi:10.2113/gsecongeo.88.6.1643.

Campbell, I.H., Lesher, C.M., Coad, P., Franklin, J.M., Gorton, M.P., and Thurston, P.C. 1984. Rare-earth element mobility in alteration pipes below massive Cu-Zn sulfide deposits. Chemical Geology, **45**: 181–202. doi:10.1016/0009-2541(84)90036-6.

Card, K.D., and Poulsen, K.H. 1998. Archean and Paleoproterozoic geology and metallogeny of the southern Canadian Shield. Exploration and Mining Geology, **7**: 181–215.

Cas, R.A.F., Allen, R.L., Bull, S.W., Clifford, B.A., and Wright, J.V. 1990. Subaqueous, rhyolitic dome-top tuff cones: a model based on the Devonian Bunga Beds, southeastern Australia and a modern analogue. Bulletin of Volcanology, **52**: 159–174. doi:10.1007/BF00334802.

Castillo, P.R., Janney, P.E., and Solidum, R.U. 1999. Petrology and geochemistry of Camiguin Island, southern Philippines: insights to the source of adakites and other lavas in a complex arc setting. Contributions to Mineralogy and Petrology, **134**: 33–51. doi:10.1007/s004100050467.

Corfu, F., Krogh, T.E., Kwok, Y.Y., and Jensen, L.S. 1989. U-Pb zircon geochronology in the southwestern Abitibi greenstone belt, Superior Province. Canadian Journal of Earth Sciences, **26**(9): 1747–1763. doi:10.1139/e89-148.

Date, J., Watanabe, Y., and Saeki, Y. 1983. Zonal alteration around the Fukazawa Kuroko deposits, Akita Prefecture, northern Japan. Economic Geology Monograph, **5**: 365–386.

Davies, J.F., and Luhta, L.E. 1978. An Archean 'porphyry-type' disseminated copper deposit, Timmins, Ontario. Economic Geology, **73**: 383–396. doi:10.2113/gsecongeo.73.3.383.

Davies, J.F. 1980. K-Rb patterns in an Archean "porphyry-type" copper deposit, Timmins, Ontario, Canada. Economic Geology, **75**: 760–770.

Davis, W.J., Lacroix, S., Gariepy, C., and Machado, N. 2000. Geochronology and radiogenic isotope geochemistry of plutonic rocks from the central Abitibi subprovince: significance to the internal subdivision and plutono-tectonic evolution of the Abitibi belt. Canadian Journal of Earth Science, **37**: 117–133. doi:10.1139/e99-093.

Defant, M.J., and Drummond, M.S. 1990. Derivation of some modern arc magmas by melting of young subducted lithosphere. Nature, **347**: 662–665. doi:10.1038/347662a0.

Dinel, E., Fowler, A.D., Ayer, J., Still, A., Tylee, K., and Barr, E. 2008. Lithogeochemical and stratigraphic controls on gold mineralization within the metavolcanic rocks of the Hoyle Pond Mine, Timmins, Ontario. Economic Geology, **103**: 1341–1363. doi:10.2113/gsecongeo.103.6.1341.

Drummond, M.S., and Defant, M.J. 1990. A model for trondhjemite-tonalite-dacite genesis and crustal growth via slab melting: Archean to modern comparisons. Journal of Geophysical Research, B, Solid Earth and Planets, **95**: 21503–21521. doi:10.1029/JB095iB13p21503.

Drummond, M.S., Defant, M.J., and Kepezhinskas, P.K. 1996. Petrogenesis of slab-derived trondhjemite-tonalite-dacite/adakite magmas. *In* The Third Hutton Symposium on the Origin of Granites and Related Rocks. *Edited by* M. Brown et al. Geological Society of America, Special Paper 315, pp. 205–215.

Dubé, B., Mercier-Langevin, P., Ayer, J., Atkinson, B., and Monecke, T. 2017. Orogenic greenstone-hosted quartz-carbonate gold deposits of the Timmins-Porcupine Camp. *In* Archean base and precious metal deposits, Southern Abitibi greenstone belt, Canada, Reviews in Economic Geology, Vol. 19, pp. 51–79.

Feng, R., and Kerrich, R. 1992. Geochemical evolution of granitoids from the Archean Abitibi Southern Volcanic Zone and the Pontiac Subprovince, Superior Province, Canada: implications for tectonic history and source regions. Chemical Geology, **98**: 23–70. doi:10.1016/0009-2541(92)90090-R.

Ferguson, S.A. 1968. Geology and ore deposits of Tisdale Township, District of Cochrane. Ontario Department of Mines, 117 p.

Gorman, B.E., Kerrich, R., and Fyfe, W.S. 1981. Geochemistry and Field Relations of lode gold deposits in felsic igneous intrusions - porphyries of the Timmins District. Ontario Geological Survey, Sudbury, Ont. Miscellaneous Paper **98**, 108–124 p.

Grant, J.A. 1986. The isocon diagram: a simple solution to Gresens' equation for metasomatic alteration. Economic Geology, **81**: 1976–1982. doi:10.2113/gsecongeo.81.8.1976.

Gray, M.D., and Hutchinson, R.W. 2001. New evidence for multiple periods of gold emplacement in the Porcupine Mining District, Timmins area, Ontario, Canada. Economic Geology, **96**: 453–475. doi:10.2113/gsecongeo.96.3.453.

Hall, L.A.F., MacDonald, C.A., and Dinel, E. 2003. Precambrian geology of Deloro Township, Preliminary Map P.3528, scale 1:20000. Ontario Geological Survey, Sudbury, Ontario, Canada.

Huston, D.L. 1993. The effect of alteration and metamorphism on wall rocks to the Balcooma and Dry River South volcanic-hosted massive sulfide deposits, Queensland, Australia. Journal of Geochemical Exploration, **48**: 277–307. doi:10.1016/0375-6742(93)90008-A.

Israr, A.W. 2017. Melt inclusion chemistry and associated Cu-Mo-Au mineralization in the 2.7 Ga porphyry intrusions and volcanics, Timmins, Ontario. Unpublished B.Sc. (Hons) thesis, St. Mary's University, 68 p.

Jiang, N., Liu, Y., Zhou, W., Yang, J., and Zhang, S. 2007. Derivation of Mesozoic adakitic magmas from ancient lower crust in the North China craton. Geochimica et Cosmochimica Acta, **71**: 2591–2608. doi:10.1016/j.gca.2007.02.018.

Ketchum, J.W.F., Ayer, J.A., van Breemen, O., Pearson, N.J., and Becker, J.K. 2008. Pericontinental crustal growth of the southwestern Abitibi subprovince, Canada – U-Pb, Hf, and Nd isotope evidence. Economic Geology, **103**: 1151–1184. doi:10.2113/gsecongeo.103.6.1151.

Large, R.R., Gemmell, J.B., Paulick, H., and Huston, D.L. 2001. The alteration box plot: a simple approach to understanding the relationships between alteration mineralogy and lithogeochemistry associated with VHMS deposits. Economic Geology, **96**: 957–971. doi:10.2113/gsecongeo.96.5.957.

MacDonald, P.J., and Piercey, S.J. 2003. 36. Discover Abitibi Gold Subproject 3. Preliminary Regional Geological Assessment of porphyry intrusions spatially associated with gold deposits in the Western Abitibi Subprovince, Timmins, Ontario. *In* Summary of field work and other activities 2003. Ontario Geological Survey, Open File 6120, pp. 36.1–36.7.

MacDonald, P.J., Piercey, S.J., and Hamilton, M.A. 2004. Discover Abitibi. Gold Subproject 3. Regional geological assessment of porphyry intrusions spatially associated with Gold Deposits along the Porcupine-Destor Deformation Zone, Western Abitibi Subprovince, Timmins, Ontario. *In* Summary of field work and other activities 2004. Ontario Geological Survey, Open File 6145, pp. 43.1–43.7.

MacDonald, P.J., Piercey, S.J., and Hamilton, M.A. 2005. Discover Abitibi Intrusion Subproject: an integrated study of intrusive rocks spatially associated with gold and base metal mineralization in Abitibi Greenstone Belt, Timmins Area and Clifford Township. Ontario Geological Survey, Sudbury, Ont. Open File 6160, 190 p.

Marmont, S., and Corfu, F. 1989. Timing of gold introduction in the late Archean tectonic framework of the Canadian Shield; evidence from U-Pb zircon geochronology of the Abitibi Subprovince. Economic Geology Monographs, **6**: 101–111.

Martin, H. 1999. Adakitic magmas: modern analogues of Archaean granitoids. Lithos, **46**: 411–429. doi:10.1016/S0024-4937(98)00076-0.

Martin, H., and Moyen, J.-F. 2002. Secular changes in tonalite-trondhjemite-granodiorite composition as markers of the progressive cooling of Earth. Geology, **30**: 319–322. doi:10.1130/0091-7613(2002)030<0319:SCITTG>2.0.CO;2.

Martin, H., Smithies, R.H., Rapp, R., Moyen, J.-F., and Champion, D. 2005. An overview of adakite, tonalite-trondhjemite-granodiorite (TTG), and sanukitoid: relationships and some implications for crustal evolution. Lithos, **79**: 1–24. doi:10.1016/j.lithos.2004.04.048.

Mason, R. 1986*a*. The McIntyre-Hollinger investigation, Timmins, Ontario; a gold dominated porphyry copper system. *In* Geological Survey of Canada. *Edited by* N. Melnik. Geological Survey of Canada, Ottawa, Ont., Canada, Canada, 86-1B, 577–583 p.

Mason, R. 1986*b*. The McIntyre-Hollinger investigation, Timmins, Ontario; stratigraphy, lithology and structure. *In* Geological Survey of Canada. *Edited by* N. Melnik. Geological Survey of Canada, Ottawa, Ont., Canada, Canada, 86-1B, 567–575 p.

Mason, R., and Melnik, N. 1986. The anatomy of an Archean gold system; the McIntyre-Hollinger Complex at Timmins, Ontario, Canada. *In* Proceedings of Gold '86: An International Symposium on the Geology of Gold. *Edited by* A.J. MacDonald, pp. 40–55.

McAuley, J.B. 1983. A Petrographic and Geochemical Study of the Preston, Preston West, and Paymaster porphyries, Timmins, Ontario. Unpublished M.Sc. thesis, Laurentian University, 118 p.

Melnik-Proud, N. 1992. The geology and ore controls in and around the McIntyre Mine at Timmins, Ontario, Canada. Unpublished Ph.D. thesis, Queen's University, 353 p.

Migdisov, A., Williams-Jones, A.E., Brugger, J., and Caporuscio, F.A. 2016. Hydrothermal transport, deposition, and fractionation of the REE: Experimental data and thermodynamic calculations. Chemical Geology, **439**: 13–42. doi:10.1016/j.chemgeo.2016.06.005.

Monecke, T., Mercier-Langevin, P., Dubé, B., and Frieman, B.M. 2017. Geology of the Abitibi greenstone belt. *In* Archean base and precious metal deposits, Southern Abitibi greenstone belt, Canada. Reviews in Economic Geology, **19**: 7–49.

Moyen, J.-F. 2009. High Sr/Y and La/Yb ratios: The meaning of the "adakitic signature". Lithos, **112**: 556–574. doi:10.1016/j.lithos.2009.04.001.

Moyen, J.-F., and Stevens, G. 2006. Experimental constraints on TTG petrogenesis; implications for Archean geodynamics. Archean Geodynamics and Environments, **164**: 149–175. doi:10.1029/164GM11.

Murphy, J.B., and Hynes, A.J. 1986. Contrasting secondary mobility of Ti, P, Zr, Nb, and Y in two metabasaltic suites in the Appalachians. Canadian Journal of Earth Sciences, **23**(8): 1138–1144. doi:10.1139/e86-112.

Pearce, J.A. 1996. A user's guide to basalt discrimination diagrams. *In* Trace element geochemistry of volcanic rocks: applications for massive sulphide exploration. *Edited by* D.A. Wyman. Geological Association of Canada, Short Course Notes Vol. 12, pp. 79–113.

Pearce, J.A., Harris, N.B.W., and Tindle, A.G. 1984. Trace element discrimination diagrams for the tectonic interpretation of granitic rocks. Journal of Petrology, **25**: 956–983. doi:10.1093/petrology/25.4.956.

Piercey, S.J., Chaloux, E.C., Peloquin, A.S., Hamilton, M.A., and Creaser, R.A. 2008. Synvolcanic and younger plutonic rocks from the Blake River Group: implications for regional metallogenesis. Economic Geology, **103**: 1243–1268. doi:10.2113/gsecongeo.103.6.1243.

Pyke, D.R. 1982. Geology of the Timmins area, District of Cochrane. Ontario Geological Survey Report, Ontario Geological Survey, Toronto, Ont., Canada, 141 p.

Rapp, R.P. 1997. Heterogeneous source regions for Archaean granitoids; experimental and geochemical evidence. Oxford Monographs on Geology and Geophysics, Vol. 35, pp. 267–279.

Rapp, R.P., Watson, E.B., and Miller, C.F. 1991. Partial melting of amphibolite/eclogite and the origin of Archean trondhjemites and tonalites. Precambrian Research, **51**: 1–25. doi:10.1016/0301-9268(91)90092-O.

Rapp, R.P., Shimizu, N., Norman, M.D., and Applegate, G.S. 1999. Reaction between slab-derived melts and peridotite in the mantle wedge: experimental constraints at 3.8 GPa. Chemical Geology, **160**: 335–356. doi:10.1016/S0009-2541(99)00106-0.

Richards, J.P., and Kerrich, R. 2007. Special Paper: Adakite-like rocks: their diverse origins and questionable role in metallogenesis. Economic Geology, **102**: 537–576. doi:10.2113/gsecongeo.102.4.537.

Robert, F., and Poulsen, K.H. 1997. World-class Archaean gold deposits in Canada: an overview. Australian Journal of Earth Sciences: An International Geoscience Journal of the Geological Society of Australia, **44**: 329–351. doi:10.1080/08120099708728316.

Ropchan, J.R., Luinstra, B., Fowler, A.D., Benn, K., Ayer, J., Berger, B., Dahn, R., Labine, R., and Amelin, Y. 2002. Host-rock and structural controls on the nature and timing of gold mineralization at the Holloway Mine, Abitibi Subprovince, Ontario. Economic Geology, **97**: 291–309. doi:10.2113/gsecongeo.97.2.291.

Ross, P.-S., and Bedard, J.H. 2009. Magmatic affinity of modern and ancient subalkaline volcanic rocks determined from trace-element discriminant diagrams. Canadian Journal of Earth Sciences, **46**(11): 823–839. doi:10.1139/E09-054.

Saeki, Y., and Date, J. 1980. Computer application to the alteration data of the footwall dacite lava at the Ezuri Kuroko deposits, Akito Prefecture. Mining Geology, **30**: 241–250. doi:10.11456/shigenchishitsu1951.30.241.

Seward, T.M. 1973. Thio complexes of gold and the transport of gold in hydrothermal ore solutions. Geochimica et Cosmochimica Acta, **37**: 379–399. doi:10.1016/0016-7037(73)90207-X.

Smithies, R.H. 2000. The Archaean tonalite-trondhjemite-granodiorite (TTG) series is not an analogue of Cenozoic adakite. Earth and Planetary Science Letters, **182**: 115–125. doi:10.1016/S0012-821X(00)00236-3.

Spitz, G., and Darling, R. 1978. Major and minor element lithogeochemical anomalies surrounding the Louvem copper deposit, Val d'Or, Quebec. Canadian Journal of Earth Sciences, **15**(7): 1161–1169. doi:10.1139/e78-122.

Sun, S.-s., and McDonough, W.F. 1989. Chemical and isotopic systematics of oceanic basalts: implications for mantle composition and processes. *In* Magmatism in the Ocean Basins. *Edited by* A.D. Saunders and M.J. Norry. Geological Society Special Publication, Vol. 42, pp. 313–345.

Thompson, P.H. 2002. Toward a new metamorphic framework for gold exploration in the Timmins area, central Abitibi greenstone belt; Ontario Geological Survey, Open File Report 6101, 51p.

Thurston, P.C., Ayer, J.A., Goutier, J., and Hamilton, M.A. 2008. Depositional gaps in Abitibi greenstone belt stratigraphy: A key to exploration for syngenetic mineralization. Economic Geology, **103**: 1097–1134. doi:10.2113/gsecongeo.103.6.1097.

Wang, Q., Wyman, D.A., Xu, J., Jian, P., Zhao, Z., Li, C., Xu, W., Ma, J., and He, B. 2007. Early Cretaceous adakitic granites in the Northern Dabie Complex, central China: Implications for partial melting and delamination of thickened lower crust. Geochimica et Cosmochimica Acta, **71**: 2609–2636. doi:10.1016/j.gca.2007.03.008.

Wells, R.C. 2001. Petrographic, lithogeochemical and interpretative report on a porphyry sample suite, Dome Mine area; internal, unpublished report for Placer Dome Limited, 32p.

Winchester, J.A., and Floyd, P.A. 1977. Geochemical discrimination of different magma series and their differentiation products using immobile elements. Chemical Geology, **20**: 325–343. doi:10.1016/0009-2541(77)90057-2.

Wood, P.C., Burrows, D.R., Thomas, A.V., and Spooner, E.T.C. 1986. The Hollinger-McIntyre Au-quartz vein system, Timmins, Ontario, Canada; geologic characteristics, fluid properties and light stable isotope geochemistry. *In* Proceedings of Gold 86: An International Symposium on the Geology of Gold Deposits. *Edited by* A.J. MacDonald, pp. 56–80.

Wyllie, P.J., Wolf, M.B., and van der Laan, S.R. 1997. Conditions for formation of tonalites and trondhjemites; magmatic sources and products. Oxford Monographs on Geology and Geophysics, Vol. 35, pp. 256–266.

Wyman, D., and Kerrich, R. 2009. Plume and arc magmatism in the Abitibi subprovince: Implications for the origin of Archean continental lithospheric mantle. Precambrian Research, **168**: 4–22. doi:10.1016/j.precamres.2008.07.008.